1999-12

# Evaluation of range compensation in thermal imaging of ships using the Eopace data base

Tsustsui, Roberto

Monterey, California ; Naval Postgraduate School

# NAVAL POSTGRADUATE SCHOOL
## Monterey, California


# THESIS

**EVALUATION OF RANGE COMPENSATION IN THERMAL IMAGING OF SHIPS USING THE EOPACE DATA BASE**

by

Roberto Tsustsui

December 1999

Thesis Advisor: Alfred W. Cooper
Thesis Co-Advisor: Ron J. Pieper

# REPORT DOCUMENTATION PAGE

Form Approved
OMB No. 0704-0188



| 1. AGENCY USE ONLY *(Leave blank)* | 2. REPORT DATE | 3. REPORT TYPE AND DATES COVERED |
|---|---|---|
| | December 1999 | Master's Thesis |

**4. TITLE AND SUBTITLE**
**EVALUATION OF RANGE COMPENSATION IN THERMAL IMAGING OF SHIPS USING THE EOPACE DATA BASE**

**5. FUNDING NUMBERS**

**6. AUTHOR(S)**
Tsustsui, Roberto

**7. PERFORMING ORGANIZATION NAME(S) AND ADDRESS(ES)**
Naval Postgraduate School
Monterey, CA 93943-5000

**8. PERFORMING ORGANIZATION REPORT NUMBER**

**9. SPONSORING / MONITORING AGENCY NAME(S) AND ADDRESS(ES)**

**10. SPONSORING / MONITORING AGENCY REPORT NUMBER**

**11. SUPPLEMENTARY NOTES**
The views expressed in this thesis are those of the author and do not reflect the official policy or position of the Department of Defense or the U.S. Government.

**12a. DISTRIBUTION / AVAILABILITY STATEMENT**
Approved for public release; distribution is unlimited.

**12b. DISTRIBUTION CODE**

**13. ABSTRACT *(maximum 200 words)***

An ever-present problem in analyzing thermal images for target signatures is the influence of atmospheric effects in the signature observed at significant range. The compensation for these effects, mostly atmospheric absorption and scattering and path radiance requires accurate knowledge of the meteorological parameters for the area involved at the time of the measurements.

Based both on infrared image files taken during the Electro-optical Propagation Assessment in Coastal Environments (EOPACE) experiment together with the EOPACE environmental data base and on the SeaRad propagation code to generate radiance, a range compensation algorithm is proposed in this thesis. Applying SeaRad output adjusted for the sky path radiance, an 11 by 11 matrix of the apparent sea temperatures is constructed in which each row corresponds to a different zenith angle and therefore range, and each column to a different sea apparent black body temperature. By interpolation all sea pixels in the image are range compensated. The ship pixels are range compensated by imposing continuity in the sea ship interface. The magnitude of scene temperature correction required is of the order of -2.3 ± 1.7 °C which is comparable to the precision of the recorded data.

**14. SUBJECT TERMS**
Infrared Radiation, Radiance, Atmospheric Propagation, Range Compensation, Thermal Imaging

**15. NUMBER OF PAGES**
92

**16. PRICE CODE**

| 17. SECURITY CLASSIFICATION OF REPORT | 18. SECURITY CLASSIFICATION OF THIS PAGE | 19. SECURITY CLASSIFI- CATION OF ABSTRACT | 20. LIMITATION OF ABSTRACT |
|---|---|---|---|
| Unclassified | Unclassified | Unclassified | UL |

NSN 7540-01-280-5500 (Rev. 2-89) Standard Form 298

Prescribed by ANSI Std. 239-18

**Approved for public release; distribution is unlimited**

# EVALUATION OF RANGE COMPENSATION IN THERMAL IMAGING OF SHIPS USING THE EOPACE DATA BASE

Roberto Tsustsui
Lieutenant Colonel, Brazilian Air Force
B.S., Technological Institute of Aeronautics, 1978

Submitted in partial fulfillment of the
requirements for the degree of

**MASTER OF SCIENCE IN APPLIED PHYSICS**

from the

**NAVAL POSTGRADUATE SCHOOL**
**December 1999**

# ABSTRACT

An ever-present problem in analyzing thermal images for target signatures is the influence of atmospheric effects in the signature observed at significant range. The compensation for these effects, mostly atmospheric absorption and scattering and path radiance requires accurate knowledge of the meteorological parameters for the area involved at the time of the measurements.

Based both on infrared image files taken during the Electro-optical Propagation Assessment in Coastal Environments (EOPACE) experiment together with the EOPACE environmental data base and on the SeaRad propagation code to generate radiance, a range compensation algorithm is proposed in this thesis. Applying SeaRad output adjusted for the sky path radiance, an 11 by 11 matrix of the apparent sea temperatures is constructed in which each row corresponds to a different zenith angle and therefore range, and each column to a different sea apparent black body temperature. By interpolation all sea pixels in the image are range compensated. The ship pixels are range compensated by imposing continuity in the sea ship interface. The magnitude of scene temperature correction required is of the order of $-2.3 \pm 1.7$ °C which is comparable to the precision of the recorded data.

# TABLE OF CONTENTS

# ACKNOWLEDGEMENT

I wish to express my gratitude to those people in the Brazilian Air Force who contributed to give me this unique opportunity to get a Masters Degree at the Naval Postgraduate School. It was a long-term full-time training that will add new academic, technical and cultural perspective in my life.

A very special thanks to Professor Alfred W. Cooper and Professor Ron Pieper for their help, patience, guidance, and many hours of counseling that have made possible this work, and if this thesis deserves some merit, it is a consequence of their dedication.

This project was conducted under partial support from the Naval Postgraduate School Institute for Joint Warfare Analysis and from Naval Sea System Command, PEO-TSC.

Finally, I would like to thank my wife Marie and my children Marcelo and Roberta for their support and comprehension in all these years of school, when many times they quench their needs and desires for the benefit of my study.

# I. INTRODUCTION

All predictive codes are based on the target-plane target signature. This poses a challenge to range-compensate target signatures for the influence of atmospheric effects and other sources of radiation.

The Electro-optical Propagation Assessment in Coastal Environments (EOPACE) database allows an evaluation of this compensation method. A very comprehensive characterization of the meteorology and sea surface parameters, including data from two Naval Postgraduate School (NPS) buoys moored in San Diego Bay, is available for the period of intensive measurements in EOPACE. Full shipboard location and local meteorology data were recorded on the R/V POINT SUR for two days of operations in the sector south of Point Loma, where NPS polarization imaging equipment was located. During these two days the POINT SUR operated in close liaison with the NPS-NACIT imaging group on the south tip of Point Loma. The POINT SUR took up stationary positions at varied aspect angle at selected ranges along several bearing lines from the images.

The purpose of this thesis was to develop a method to compensate the imagery for the atmospheric extinction and radiance effects. But, to check the correctness of the method more than just the thermal image data is necessary. The NPS Boundary Layer group played that role, supplying meteorological and geographical data.

A usual approach to range-compensate a thermal image is to begin by finding the equivalent radiance, here called the "full range radiance", for each pixel value in the image plane (that is, for each apparent temperature). With this full range radiance and calculating the atmospheric transmittance and path radiances using SeaRad (a computer code that calculates transmittance and path and sea radiance), the radiance at the source plane (zero range radiance) can be calculated and also the corresponding zero range apparent temperature (the range-compensated temperature). SeaRad is a rigorous geometric capillary wave model based on the Cox and Munk wave-slope statistical model suitable for moderate wind, high altitude, slant-path sensor configurations, that was developed by Naval Command Control and Ocean Surveillance Center (NCCOSC), now Spawar Systems Center, San Diego.

But this approach is very arduous and computer time-consuming and in consequence a new method is presented in this thesis. Basically, using SeaRad, a matrix of apparent sea temperatures at full range with dimensions eleven by eleven is built first, in which each column corresponds to different arbitrary apparent sea temperatures at zero range and each row

corresponds to different arbitrary zenith angle. Then, for each row of sea pixels at the image plane the corresponding zenith angle is calculated. Using two rows of that matrix, a new matrix with dimensions one by eleven is interpolated for that zenith angle, but which keeps the same column correspondence of the previous matrix. Finally, for each sea pixel value (that is, each apparent temperature at full range), the apparent temperature at zero range can be found by interpolation, using the one by eleven matrix. For the ship the process is the same except that the base matrix has dimensions one by eleven because all ship pixels have the same zenith angle.

This thesis begins by first finding the calibration curve for the AGA equipment and for the conditions of the time of the experiment. With this curve, all image data were mapped from a digital level unit, that is characteristic of the equipment, to temperature. This image represents an apparent temperature resulting from the interaction of different sources of radiation.

The interactions of radiation from the various sources are explored in Chapter III.

In Chapter IV, the available input data are presented and analyzed. Also, other necessary inputs are determined. Those are the horizon position, the sun position, the target position, etc.

The core of this work is in Chapter V. First, the structure and the mathematical treatment applied to the data in this thesis are presented. Second, the SeaRad results are adjusted for the sky path radiance by making the calculated SeaRad apparent temperature at the horizon zenith angle to be equal to the measured horizon apparent temperature. It is found that no SeaRad correction is necessary for the sea other than the sky path correction. Finally, the range compensation method is introduced.

The conclusions and recommendations are presented in Chapter VI.

# II. EOPACE DATA

In the Electro-optical Propagation Assessment in Coastal Environments (EOPACE) experiment conducted on April 9 and April 10 of 1996 in San Diego, a set of polarized and unpolarized thermal images were taken. The Naval Postgraduate School (NPS) Boundary Layer Meteorology Group and the NPS Center for Infrared Technology (NACIT) also have contributed to that specific EOPACE experiment by recording meteorological and geographical data. In [Ref.7] and [Ref. 8] there is a complete description of the experiment with characterization of the experiment location, recording format and so on.

The experiment can be represented diagrammatically by Figure 2. 1, where an observer (sensor) receives an image attenuated during its propagation through the atmosphere. The observer has also available recorded meteorological and geographical data that would allow him to analyze thermal vision images.

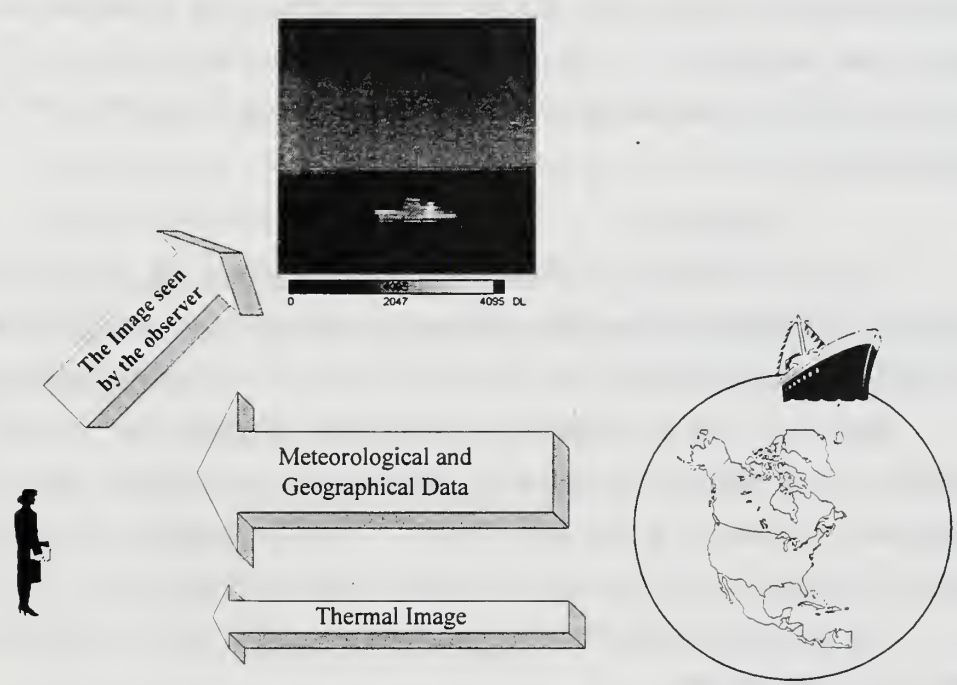


Figure 2. 1 The EOPACE Experiment.

In the experiment of April 9 and April 10 of 1996 the following parameters were kept invariant:

- The observer geographic coordinates (also called sensor or camera position in this document): 32° 39' 55" N, 117° 14' 31".
- The instrumentation: AGA 780 Thermovision System.
- The target: R/V POINT SUR: a 135 foot long ship.

The variant parameters were:

- The ship position relative to the observer.
- The ship heading.
- The uncontrollable ship signature and sea temperature.
- The Sun position.
- The uncontrollable weather conditions: wind intensity and direction, relative air humidity, air temperature, and air pressure.

## A. INVARIANT PARAMETERS

The fact that the same AGA 780 Thermovision System equipment was used during the whole experiment does not mean that the instrumentation is not adding any sort of additional error to the measurements. Two elements can have a great influence on the results: the equipment calibration and the equipment drift. Another kind of error that could be significant is operator error.

### 1. Calibration

The use of different controller units does not affect the results of thermal image acquisition, but different scanners have different calibration curves and will affect the output. In the experiment the scanner used was: AGA serial number 5016, locally called "the NOSC head".

Since there was no calibration curve directly associated with the data taken in this experiment, it is necessary to determine experimentally a calibration curve and check the differences in relation to a past determination. Then, the calibration curve found should be applied to the experimental data in order to figure out the magnitude of error, if it exists.

The comparison calibration curve used was one made by E.C. Crittenden on March 21, 1996 on the same scanner.

For the calibration determination of this thesis the following settings and equipment were used:

- Scanner serial number 5016.
- Acquisition software: PTRWIN.

- Black body standard source Graseby Infrared, Inc. model 140/201
- 7° FOV lens;
- The Black Body distance from the lens is 1 meter.

The PTRWIN program [Ref. 12] is an acquisition and analysis software package that uses a 12 bit Analog-to-digital converter for converting the detector signal intensity into a real-time image on a computer screen and for digital image recording. PTRWIN has two functions that are very useful in analyzing images: the spot and the area options. The spot option of the PTRWIN software allows measuring spots of a displayed image, and the area option to calculate the statistics for selected areas of the screen.

The following procedure was adopted for reading the AGA temperature corresponding to the Black body temperature:

- Use the spot and area options of the PTRWIN software to read the correct value of the output in isothermal units (IU).
- Adjust the thermal level dial until saturation of the highest temperature color occurs. At this time the thermal level value presented at the spot camera dialog window will be the same as the maximum IU value displayed in the color bar representation of the image (saturation). From that point on, it will stay constant if the thermal level is decreased, but the IU value will also decrease, showing that the recorded value was the maximum.

### *a. Black Body Characterization*

The black body used in the calibration experiment conducted in the laboratory has the following specifications:

- Temperature range: ambient to 230 °C.
- Absolute calibration accuracy: ± 1.5 °C.
- Stability: ± 1 °C.
- Resolution: 1 °C.
- Cavity opening: 12"x12" square.
- Temperature distribution: approximately 2 °C edge to edge.
- Cavity emissivity: 0.95 ± 2%.

A flat-top profile of temperature along the vertical and horizontal axes of the black body cavity is desired. To verify this surface uniformity, the temperature distribution along

the vertical axis (1) and along the horizontal axis (2) of the black body at 80 °C are shown in Figure 2. 2.

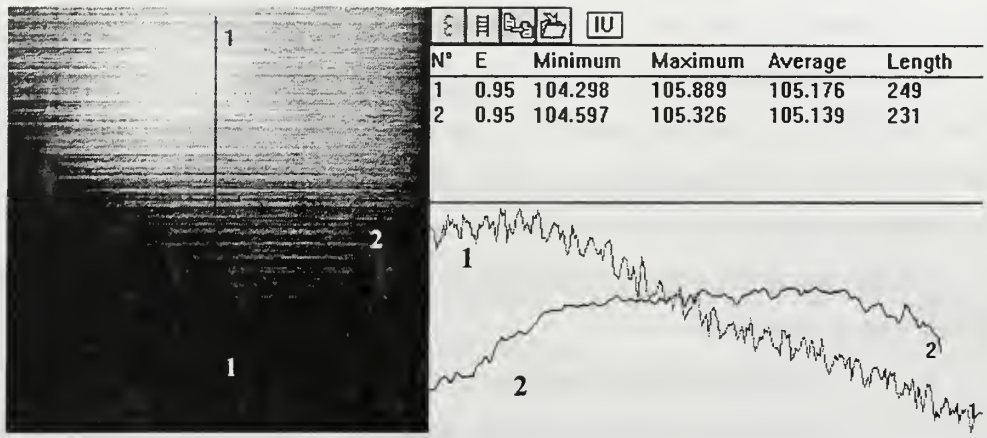


Figure 2. 2 Temperature distribution on the Black Body Cavity at 80 °C.

Note that the horizontal axis has better uniformity than the vertical. Also note that the maximum and minimum values for both curves are not far apart, confirming the uniformity of the black body.

***b. Calibration Determination***

Data for three different filters were measured. Filter 6 is unpolarized, filter 5 is vertically polarized and filter 4 is horizontally polarized. Table 2. 1 presents those data for an ambient temperature of 17 °C.

| Black Body Temperature | Filter | | |
|---|---|---|---|
| (°C) | 6 | 5 | 4 |
| 23 | 51 | 50 | 50 |
| 27 | 53 | 51 | 51 |
| 33 | 58 | 52 | 52 |
| 37 | 61 | 54 | 54 |
| 43 | 66 | 57 | 57 |
| 50 | 72 | 59 | 59 |
| 61 | 82 | 63 | 63 |
| 70 | 92 | 67 | 67 |
| 80 | 103 | 71 | 71 |
| 90 | 115 | 75 | 75 |
| 100 | 128 | 80 | 80 |
| 110 | 141 | 86 | 86 |

Table 2. 1 Calibration Data for Ambient Temperature of 17 °C.

Usually the calibration curve is described by the curve-fit equation:

$$IU = \frac{A}{C \bullet e^{\frac{B}{T}} - 1} \qquad (2.\ 1)$$

Where:

- T is degrees Kelvin.
- A, B and C are constants that are found from curve fitting.

Using Mathcad 8 software, the following constants for the unpolarized case were found:

- A = 418.751
- B = 1115.0
- C = 0.216

And, for the polarized cases (filter 5 and 4):

- A = 5.679
- B = 57.46
- C = 0.918

To see the influence of ambient temperature on the isothermal values for the unpolarized filter, another set of measurements was taken at an ambient temperature of 23.4 °C with the results presented in Table 2. 2. No significant discrepancies are noted.

| **Black Body Temperature** | **Filter 6** | | | |
|---|---|---|---|---|
| 22 | 51 | 51 | 52 | 51 |
| 27 | 55 | 54 | 55 | 56 |
| 32 | 59 | 59 | 60 | 59 |
| 37 | 63 | 63 | 62 | 63 |
| 42 | 68 | 68 | 67 | 67 |
| 50 | 75 | 74 | 75 | 74 |
| 60 | 84 | 83 | 84 | 84 |
| 70 | 94 | 94 | 94 | 93 |
| 80 | 103 | 104 | 103 | 103 |
| 91 | 115 | 115 | 115 | 116 |
| 101 | 126 | 127 | 127 | 127 |
| 111 | 139 | 139 | 139 | 139 |

Table 2. 2 Calibration Data for Ambient Temperature of 23.4 °C.

The calibration constants for the average IU values are:

- A = 2318
- B = 1218
- C = 0.742

### c. *Previous NPS Calibration*

Previous NPS calibration of the AGA-780 over the time interval from 1990 to 1996 were made mostly by Dr. E. C. Crittenden and were expressed in terms of the curve fit equation incorporated in the CATS acquisition and processing software (see Equation 2.2). These calibrations are referred to in this thesis as the Crittenden calibrations.

$$IU = \frac{A}{C \bullet e^{\frac{B}{T}} - 1} + OS \qquad (2.2)$$

Where: *OS* is offset.

The calibration constants for Equation 2.2 and the corresponding values for Equation 2.1 are reported in Table 2. 3:

| Filter | Calibration Constant | Equation 2.2 | Equation 2.1 |
|---|---|---|---|
| 4 and 5 | A | 1675 | 0.36 |
| | B | . 1348 | 3.093 |
| | C | 1 | 0.996 |
| | OS | 39 | - |
| 6 | A | 6808.8 | 467.936 |
| | B | 1511 | 1101 |
| | C | 1 | 0.237 |
| | OS | 12 | - |

Table 2. 3 Crittenden Calibration Constants.

### *d. Comparison Between Crittenden Calibration and New Calibration*

For comparison purposes, in Figure 2. 4 and Figure 2. 5, the Crittenden calibration was plotted together with the new calibration for the polarized and unpolarized cases respectively. The data agree in shape but there is a non-constant offset between the data. This offset is a characteristic of the scanner controller and can be adjusted by rotating the thermal level adjustment screw located on the front chassis (number 11 in Figure 2. 3).

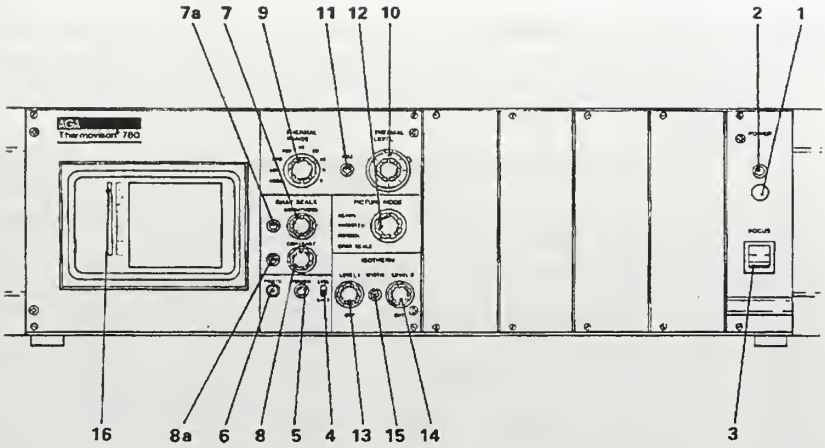


1. POWER
2. LED
3. FOCUS
4. LINE/BATT
5. POWER LED
6. PHOTO
7. BRIGHTNESS
7a. BRIGHTNESS PRESET
8. CONTRAST
8a. CONTRAST PRESET
9. THERMAL RANGE
10. THERMAL LEVEL
11. THERMAL LEVEL ADJ.
12. PICTURE MODE
13. ISOTHERM LEVEL 1
14. ISOTHERM LEVEL 2
15. ISOTHERM WIDTH
16. ISOTHERM SCALE

Figure 2. 3 AGA-780 Controller Front Panel.

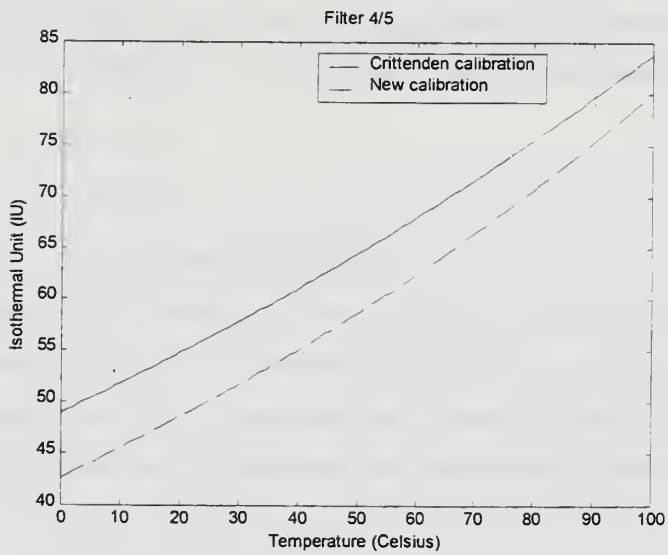


Figure 2. 4 Calibration Comparison for Polarized Filters.

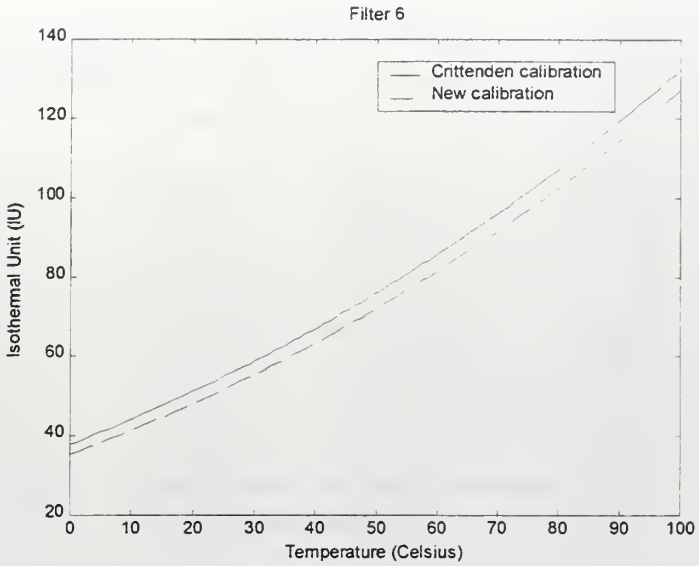


Figure 2. 5 Calibration Comparison for Unpolarized Filter.

This offset would not be serious for analysis of field data if there were calibration- checking data (a black body at a known temperature) in the recorded scene data that could allow determining the correct calibration curve. This calibration determination could be done, first, by finding the isothermal unit $IU_{ref}$ corresponding to the calibration-check black body temperature $T_{ref}$. Second, in the laboratory try to minimize the offset for that particular point ($IU_{ref}$ , $T_{ref}$) by rotating the screw located on the front panel of the controller (number 11 in Figure 2. 3). Finally, find the calibration parameters as explained in this subsection.

Note that to assume that one curve is just the offset of the other can result in high error. For example, assume that an offset between the two curves were found for 19.19 °C. Also assume that the correct curve is the new calibration. The offsetting of the entire Crittenden calibration curve by a constant amount in order to match its curve with the new calibration at 19.19 °C is represented in Table 2. 4 and Table 2. 5. In the same tables the difference in temperature for each IU is presented. These errors in the temperature scale can be seen in Table 2. 4 and Table 2. 5.

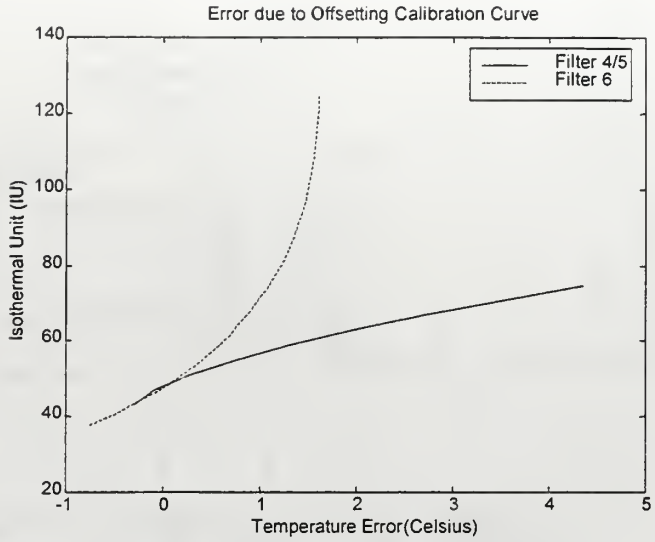


Figure 2. 6 Temperature Error Using Offset Method.

| Isothermal Unit (IU) | Crittenden Offset Temperature (°C) | Correct Temperature (°C) | Temperature Error (°C) |
|---|---|---|---|
| 45.4749 | 9.5225 | 9.7249 | 0.2024 |
| 46.1892 | 11.9764 | 12.1362 | 0.1598 |
| 48.3321 | 19.1919 | 19.1919 | 0 |
| 51.9035 | 30.753 | 30.3943 | -0.3586 |
| 55.4749 | 41.7702 | 40.9527 | -0.8175 |
| 59.0464 | 52.2806 | 50.9219 | -1.3588 |
| 62.6178 | 62.3183 | 60.3497 | -1.9685 |
| 66.9035 | 73.7837 | 71.0085 | -2.7752 |
| 71.1892 | 84.6615 | 81.0156 | -3.6459 |
| 77.6178 | 99.9731 | 94.9294 | -5.0437 |

Table 2. 4 Temperature Error for Polarized Filters - Offset Method.

| Isothermal Unit (IU) | Crittenden Offset Temperature (°C) | Correct Temperature (°C) | Temperature Error (°C) |
|---|---|---|---|
| 37.5257 | 4.389 | 3.636 | -0.7531 |
| 40.8591 | 9.5507 | 9.0837 | -0.4670 |
| 47.5257 | 19.1919 | 19.1919 | 0 |
| 57.5257 | 32.2742 | 32.7931 | 0.5188 |
| 67.5257 | 44.0682 | 44.9575 | 0.8893 |
| 77.5257 | 54.8503 | 56.0045 | 1.1542 |
| 87.5257 | 64.808 | 66.1493 | 1.3414 |
| 97.5257 | 74.0756 | 75.5454 | 1.4698 |
| 107.5257 | 82.7559 | 84.3051 | 1.5492 |
| 117.5257 | 90.9258 | 92.5165 | 1.5907 |

Table 2. 5 Temperature Error for Unpolarized Filter - Offset Method.

Then, by first finding a better calibration curve as described in the beginning of this sub-subsection and then offsetting it (if another adjustment is needed), the total error can be minimized.

But a quick look over the files of the experiment will show that there is only one black body measurement recorded, which used filter 4 and was made at the end of the day 10 April 1996. In consequence, although still not ideal, this thesis will be based only on this April 10, 1996 data, assuming that neither an operational error nor an equipment drift happened in the proximity of the time of the black body measurement.

#### *e. Data for Calibration Checking*

The data measurement for calibration checking was recorded on the file "NSFA1093.ptw", using horizontal polarization, and the black body set to 40 °C. A check of the data quality is needed knowing that the better the "flatness" of the black body the better the quality of the measurement. The method depends on the width of the feature being greater than that required for the response to rise to its maximum value. In Figure 2. 7 the temperature profiles for the horizontal plane (1) and for the vertical plane (2) across the black body are shown. The black body response is not as flat in the horizontal plane showing that a statistical evaluation over a specific area of the black body surface is needed. This can be done using the area option of PTRWIN.

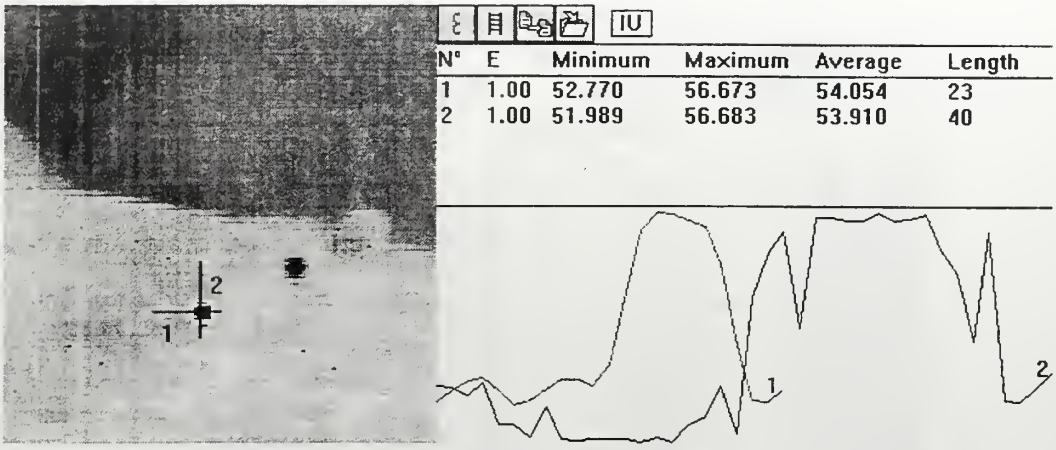


Figure 2. 7 Quality of Black Body Measurement.

Applying the area function of the PTRWIN software as shown in Figure 2. 8, the IU value corresponding to a temperature of 40 °C is 56.524 ± 0.148 IU.

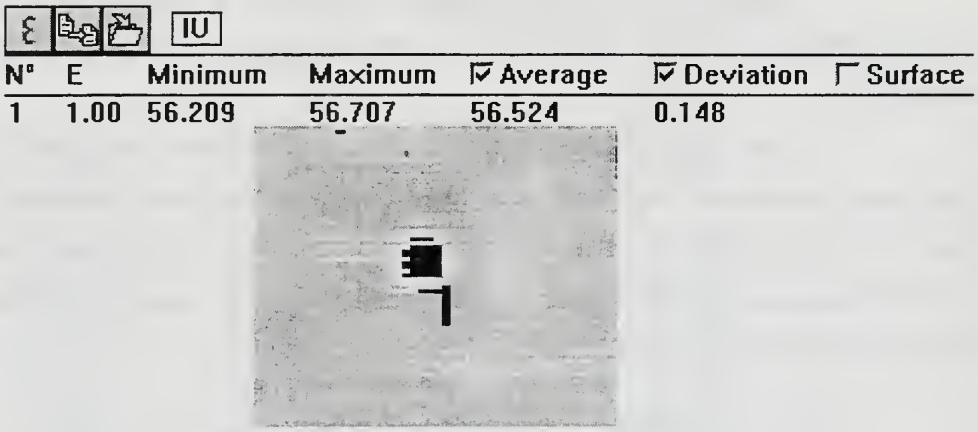


Figure 2. 8 Isothermal Unit Value for a Black Body at 40 °C.

### *f. Digital Level to Isothermal Unit*

All EOPACE images were recorded in the digital level format. In consequence, for further image analysis it is necessary to determine the relation between the digital level and the isothermal unit value.

The digital level (D) ranges from 0 to 4095 (12 bits scale) and the isothermal unit from $\left(TL-\frac{TR}{2}\right)$ to $\left(TL+\frac{TR}{2}\right)$, where TL is the thermal level and TR is the thermal range. Both data are recorded in the image headers.

Applying linear correspondence:

$$IU = TL - \frac{TR}{2} + \frac{TR \bullet D}{4{,}095} \tag{2. 3}$$

***g. The Correct Determination of Calibration Curve***

Knowing ($IU_{ref}$ , $T_{ref}$) ≡ (56.524 ± 0.148 IU, 40 °C ), and setting a black body at 40 °C, it should be easy to adjust the controller to provide an output of≈ 56.524 by rotating the screw located on the front panel of the controller, and then find the correct calibration curve. Fortunately, the (56.524 ± 0.148 IU, 40 °C ) point matches with the data collected on Table 2. 1, and in consequence Table 2. 1 contains the points of the correct calibration curve. Also, apparently no big changes have occurred in the AGA system since the end of April 1996 EOPACE experiment.

The relationship of the IU values to apparent temperature can be expressed in the calibration equation used in the PTRWIN software, namely:

$$IU = \frac{\varepsilon \bullet R}{e^{\frac{B}{T}} - F} + \frac{(1-\varepsilon) \bullet R}{e^{\frac{B}{V}} - F} \tag{2. 4}$$

Where:

- T is the object temperature in degrees Kelvin.
- ε is the object emissivity.
- V is the background temperature in degrees Kelvin.
- R, B and F are constants that are found from curve fitting.

The constants in the PTRWIN equation can be related directly to the CATS calibration constants as follows.

In the case in which the scanner field of view is smaller than the black body surface, no background is seen by the scanner and V = T in Equation 2.4, thus:

$$IU = \frac{R}{e^{\frac{B}{T}} - F} = \frac{\frac{R}{F}}{\frac{1}{F} \bullet e^{\frac{B}{T}} - 1} \tag{2. 5}$$

Comparing Equation 2.1 and Equation 2.5 for the polarized case:

$$F = \frac{1}{C} = 1.0893 \tag{2. 6}$$

$$R = A \bullet F = 6.186 \tag{2. 7}$$

And for the unpolarized case:

$$F = \frac{1}{C} = 4.630 \tag{2. 8}$$

$$R = A \bullet F = 1{,}938.662 \tag{2. 9}$$

Using the above calibration constants in PTRWIN and applying the results to the file "NSFA1093.ptw", a temperature of 42.8 ± 0.4 °C can be found for the apparent black body temperature. Again, the area function of the PTRWIN software is used as shown in Figure 2. 9.

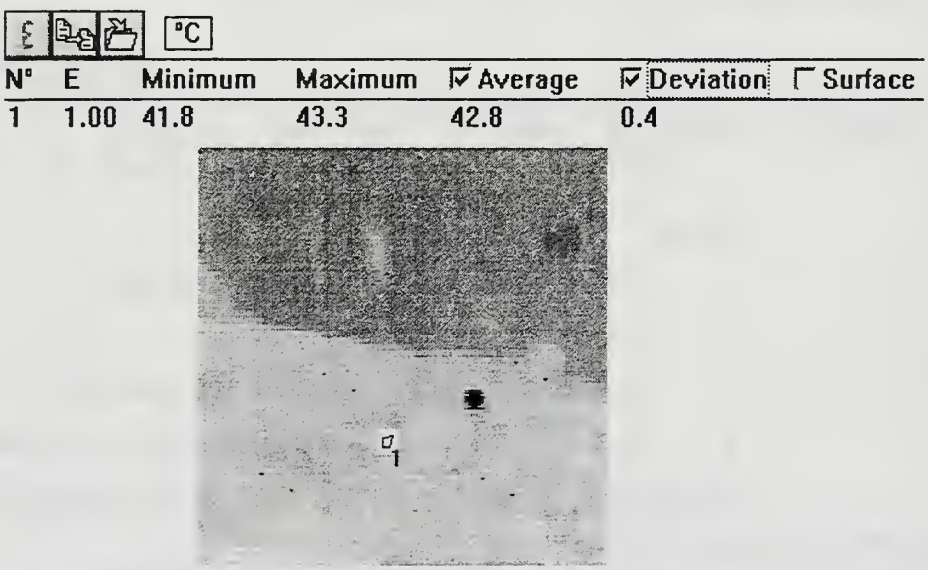


Figure 2. 9 Black Body Temperature Check.

It may be inferred that the error associated with the polarized calibration curve is +2.8± 0.4 °C.

Since there is no black body measurement for the unpolarized case on the experiment date, some black body measurements recorded in the preparation phase of the

experiment were used. All these data were recorded on April 6, 1996, using a black body at 40 °C and filter 6. The results are tabulated in Table 2. 6.

| File Name | Measured Black Body Temperature in °C |
|---|---|
| NSCA0307.ptw | 35.1 ± 0.2 |
| NSCA0314.ptw | 38.4 ± 0.1 |
| NSCA0339.ptw | 39.2 ± 0.2 |
| NSCA0342.ptw | 38.1 ± 0.1 |

Table 2. 6 Black Body Temperature for Filter 6.

Then, the average error associated with the measured unpolarized calibration curve can be found using Table 2. 6 to be -2.3 ± 1.7 °C.

***h. Influence of Temperature***

In the above calibration curves, the temperature inside the scanner was not recorded, but it will expected to be near the ambient temperature, since the experiment can be considered as a case of steady state. But to see the effect of temperature on the calibration parameters extreme conditions are needed. The conditions required were determined experimentally in the drift test described in the Subsection 2 that follows.

Note that the calibration curves measured in the laboratory for the three widely different temperatures are shown plotted together in Figure 2. 10. Although these wide variations in the laboratory produce observable changes in the calibration curve, such temperature variations would not occur in field measurements. So the calibration variation (Figure 2. 5) cannot be attributed to the ambient temperature.

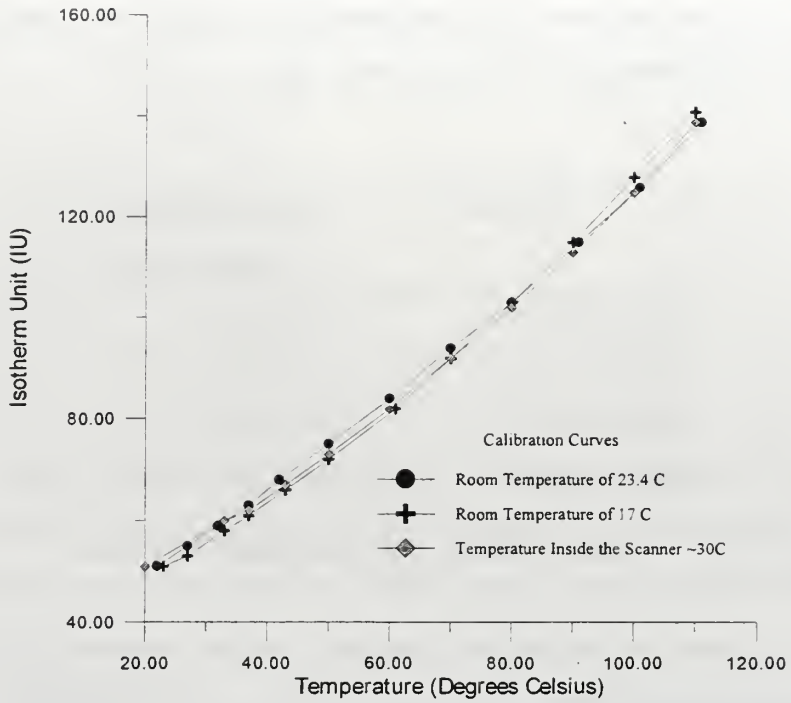


Figure 2. 10 The Temperature Effect on Calibration Curves.

**2. Drift**

To check the drift of the system, the output of a scanner radiated with a 195 °C source was monitored as depicted in Figure 2. 11.

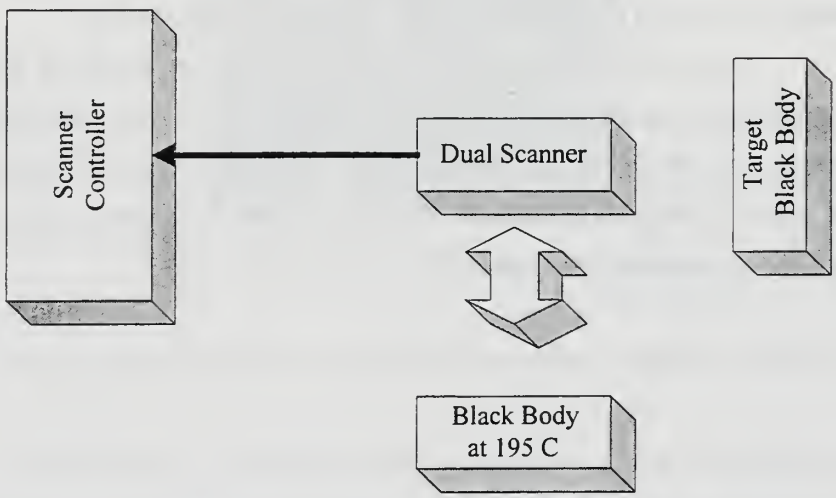


Figure 2. 11 Layout of the Drift Experiment.

Because the black body model 140/201 can be set to a temperature that ranges from zero to 230 °C, one black body was used just as a heater source.

During the whole experiment the target temperature was kept constant at 20 °C, and a thermistor was installed inside the chassis of the dual scanner, between the two dewars.

The results are contained on Table 2. 7. The drift test was stopped when the temperature inside the scanner dropped with the addition of Liquid Nitrogen (LN), because at this condition the system was in steady state.

| **Time (hh:mm)** | **Ambient Temperature ( °C )** | **Temperature Inside the Scanner ( °C )** | **Target Temperature ( °C )** | **Filter 6 (IU)** | **Note** |
|---|---|---|---|---|---|
| 02:10 | 18.1 | 16.5 | 20 | - | |
| 02:20 | 18.2 | 17.8 | 20 | 48.7 | |
| 02:25 | 18.3 | 19.3 | 20 | 48.9 | |
| 02:55 | 18.3 | 24.0 | 20 | 49.8 | |
| 02:58 | 18.3 | 24.7 | 20 | 48.9 | After adding LN |
| 03:10 | 18.3 | 27.2 | 20 | 50.9 | |
| 03:28 | 18.3 | 29.1 | 20 | 51.9 | |
| 03:33 | 18.4 | 29.3 | 20 | 50.9 | After adding LN |
| 03:49 | 18.5 | 30.0 | 20 | 50.9 | |
| 03:52 | 18.5 | 29.6 | 20 | - | After adding LN Then, near steady state. |

Table 2. 7 Drift Test Results: Observed IU Values Versus System Internal Temperature.

Note that the drift is significant when the LN level in the dewer is low. This is an operator error that could easily happen in a field experiment.

Also the maximum drifting error for this extreme ambient condition was only 2 IU. In terms of temperature this corresponds to approximately 2 °C, considering that the variation of IU is related to the variation of temperature by: $\frac{\Delta(IU)}{\Delta(T)} \cong 1$.

Using this experimental apparatus, a calibration data set was collected for this extreme ambient condition, and is shown in Table 2. 8. This calibration curve can be used to check the influence of temperature on the calibration constants (see Figure 2. 10).

| Temperature Inside the Scanner ( °C ) | Target Temperature ( °C ) | Filter 6 (IU) | Note |
|---|---|---|---|
| 30.0 | 20 | 50.9 | |
| 30.0 | 27 | 51 | |
| 30.4 | 33 | 60 | |
| 29.4 | 37 | 62 | after adding LN. |
| 29.9 | 43 | 67 | after adding LN. |
| 29.0 | 50 | 73 | after adding LN. |
| 29.5 | 60 | 82 | after adding LN. |
| 29.0 | 70 | 92 | after adding LN. |
| 29.7 | 80 | 102 | |
| 29.2 | 90 | 113 | after adding $N_2$ |
| 28.8 | 100 | 125 | after adding $N_2$ |
| 29.2 | 110 | 139 | |

Table 2. 8 Calibration Data for a Temperature Inside the Scanner of ≈ 30 °C.

### 3. Operator Error

All the images were recorded with the AGA scanner equipped with the 3.5° lens. This field of view of 3.5° is input manually by the operator and is recorded in the file header of the images. Even though it does not modify the measurement results it does influence the choice of the correct calibration curve and it effects the geometry of the image seen by the observer.

#### *a. Influence of Lens FOV on Calibration*

To see the magnitude of the error of choosing the wrong calibration curve, the calibration performed on contract by Al Fudali in April 1990 for the scanner Serial Number 4011 and for two different lenses have been plotted on the same scale in Figure 2. 12.

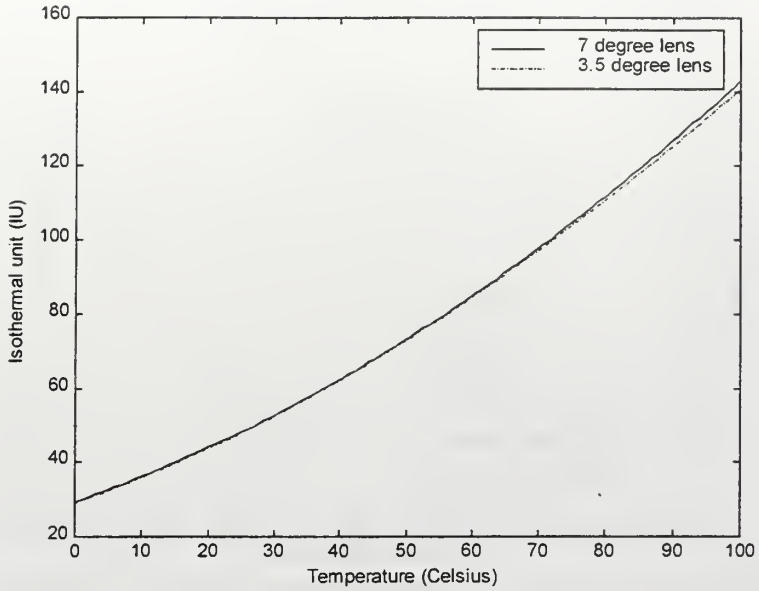


Figure 2. 12 Calibration Curves for Two Different Lens.

The error in assuming one field of view in place of another is less than 0.5 IU in the region of temperature below 60 °C, as seen in Figure 2. 13. In consequence the calibration curve for a 7° lens can be used instead of 3.5° lens without perceptible error. However the pixel dimensions will be considerably different.

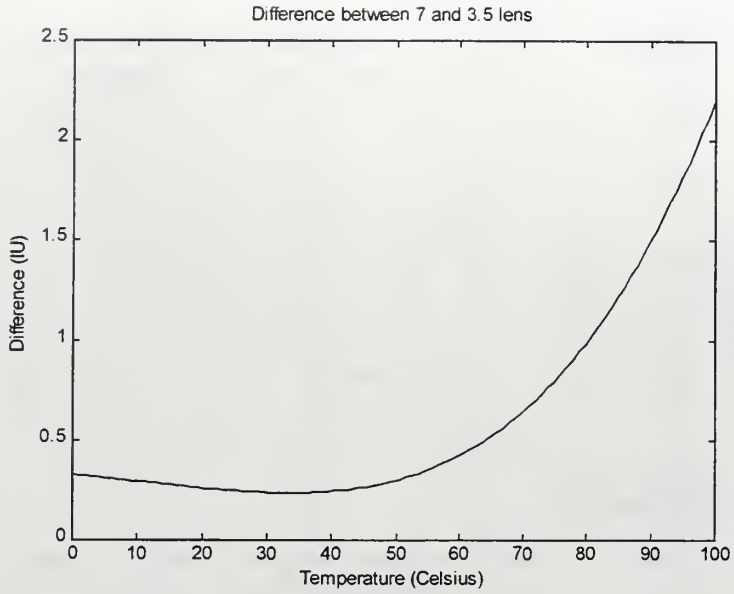


Figure 2. 13 Difference in the Calibration Values for Two Different Lenses (2-5 μm, and 8-12 μm).

### *b. Influence of Lens FOV on Geometry*

The main effect of the field-of-view (FOV) on geometry is in the image size and the relation of the pixel locations to range (FOV is the angle in Fig 2.15). Because the range will impact greatly the attenuation of radiation throughout the atmosphere, it is necessary to provide a procedure to verify the correct FOV. Since what is needed is just an estimate, the earth can be assumed spherical and we can adopt the geometry of Figure 2. 14.

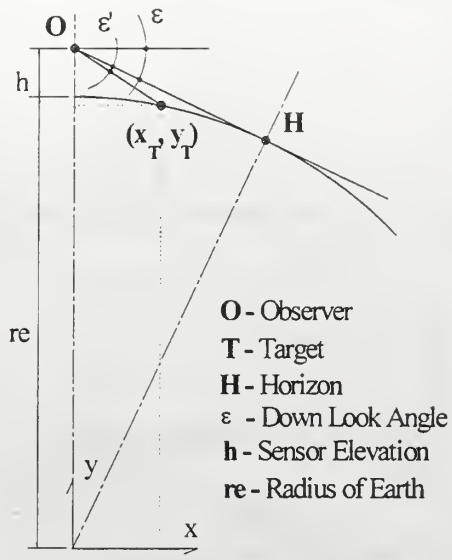


Figure 2. 14 Range Corresponding to the Down Look Angle to Sea Surface from Sensor Elevation.

From the point of view of the sensor, it sees the geometry of Figure 2. 15.

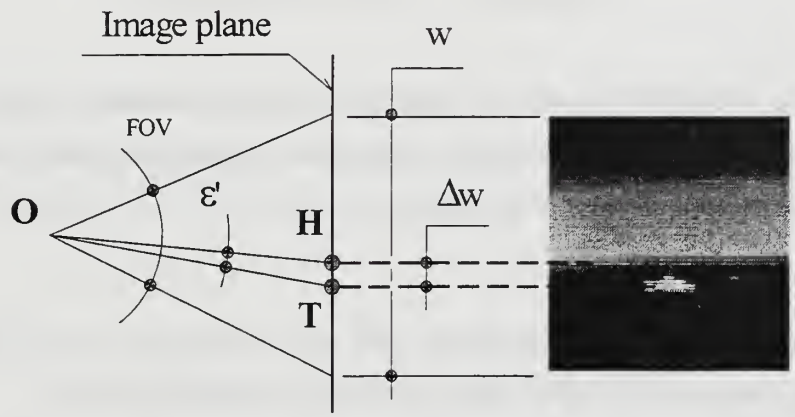


Figure 2. 15 Image Plane Geometry.

From Figure 2. 15:

$$\varepsilon' = tan^{-1}\left(\frac{\Delta w}{w} \bullet tan\, FOV\right) \tag{2. 10}$$

And from Figure 2. 14 we obtain the down look angle:

$$\varepsilon = \cos^{-1}\left(\frac{re}{re+h}\right) \tag{2. 11}$$

The point "T" , coordinates $(x_T, y_T)$ in Figure 2.14, is the solution of the following system:

$$\begin{cases} x^2 + y^2 = re^2 \\ y = (re+h) - x \bullet \tan(\varepsilon + \varepsilon') \end{cases} \tag{2. 12}$$

Thus, using Mathcad symbolic menu:

$$x_T = \frac{(h+re)\bullet \tan(\varepsilon+\varepsilon') - \sqrt{re^2 \bullet \tan(\varepsilon+\varepsilon')^2 - 2\bullet re \bullet h - h^2}}{1+\tan(\varepsilon+\varepsilon')^2} \tag{2. 13}$$

$$y_T = \frac{h+re+\tan(\varepsilon+\varepsilon')\bullet \sqrt{re^2 \bullet \tan(\varepsilon+\varepsilon')^2 - 2\bullet re \bullet h - h^2}}{1+\tan(\varepsilon+\varepsilon')^2} \tag{2. 14}$$

For small $h$, $x_T$ is a good estimate for the distance from the observer to the target, and Equation 2.13 can be used in comparison with the geographical data collected and to check the correctness of the FOV information.

## B. VARIANT DATA

Meteorological and geographical data were recorded by the NPS Boundary Layer Meteorology Group and the NPS Center for Infrared Technology (NACIT).

Sixteen thermistors were installed on the target ship at the locations shown in Figure 2. 16. The file "skindata.pte" contains those data for April 9 and 10, 1996. The data were sequentially recorded at a 20 seconds rate, where the first datum is the time in seconds in Pacific Standard Time, followed by the 16 measured temperatures from the 16 thermistors. There are two blocks of data with time varying from 0 to 86,400 seconds. The first block corresponds to April 9 and the second block to April 10.

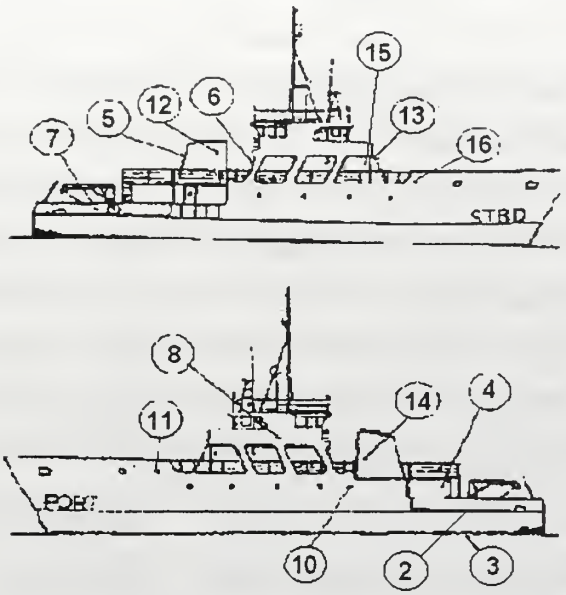


Channel # Location

| | |
|---|---|
| 1 | Reference 25.0 C |
| 2 | Aft Port |
| 3 | Aft Water Probe |
| 4 | Aft of Stack |
| 5 | Aft on Stack |
| 6 | Aft Boathouse |
| 7 | Aft Starboard |
| 8 | Port Boathouse |
| 9 | Reference 25.0 C |
| 10 | Port Below Stack |
| 11 | Port Bow |
| 12 | Starboard Stack |
| 13 | Air |
| 14 | Port Stack |
| 15 | Bow Boathouse |
| 16 | Starboard Boathouse |

Figure 2. 16 Location of Thermistors.

The remaining data are recorded on the file "eop30sec.101", usually referred to as a METOC data file. This file holds only data from April 10 and contains 25 columns of distinct information. The METOC data needed for this thesis are those included in Table 2. 9.

| Column Number | Description | Format |
|---|---|---|
| 04 | Hours and minutes (GMT) | hhmm |
| 05 | Seconds (GMT) | sss |
| 10 | True Wind Speed, m/s | mmm |
| 11 | True Wind Direction, degrees | ddd |
| 12 | Air Temperature, °C | tt.t |
| 13 | Relative Humidity, % | pp |
| 14 | Air Pressure, millibars | pppp.p |
| 15 | Sea Surface Temperature, °C | tt.t |
| 21 | Ship Latitude, degrees-minutes | ddmm.m |
| 22 | Ship Longitude, degrees-minutes | ddmm.m |

Table 2. 9 Experiment Meteorological and Geographical Data.

# III. INFRARED RADIATION

From direct viewing of a thermal image, it is hard to identify the modification that the radiance of each different source had suffered on its path to the sensor (camera). Taking the Electro-optical Propagation Assessment in Coastal Environments (EOPACE) images as an example, they have as sources of radiation: the sun, the sky vault, the sea, the target (ship), and the atmosphere. The radiation leaving each of these sources can be attenuated, reflected, or scattered by other sources. Also the attenuation depends on the distance that the radiation had traversed and is also a function of the atmosphere model. The sun component depends on the sun position relative to the sensor, the sun reflected on the sea depends on the sea wavelets, and other complexities add up to make the range compensation of a thermal image very arduous.

## A. TERMINOLOGY

The radiation leaving a small area element of source can be represented as in Figure 3. 1

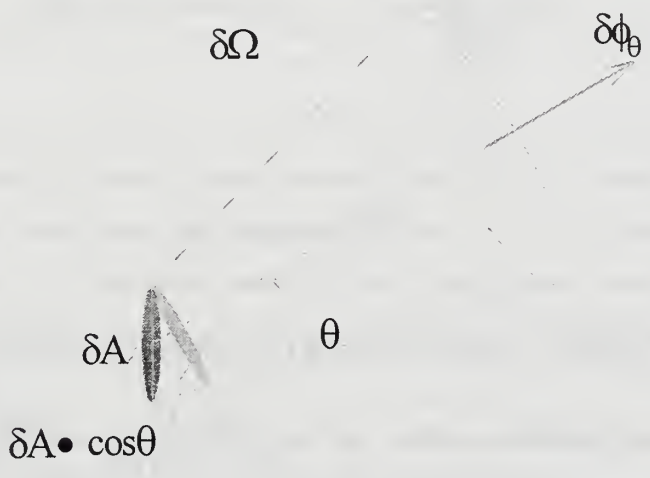


Figure 3. 1 Radiation Leaving an Area Element.

The following terminology can be defined [Ref. 1] and [Ref. 3]:

- Radiant Flux = $\delta\phi_\theta \rightarrow watts$
- Radiant Exitance or Irradiance = $M_\theta = \dfrac{\delta\phi_\theta}{\delta A \bullet \cos\theta} \rightarrow \dfrac{watts}{cm^2}$
- Radiant Intensity = $I_\theta = \dfrac{\delta\phi_\theta}{\delta\Omega} \rightarrow \dfrac{watts}{sr}$

- Radiance = $L_\theta = \dfrac{\delta I_\theta}{\delta A \bullet \cos\theta} = \dfrac{(\delta\phi_\theta)^2}{\delta A \bullet \cos\theta \bullet \delta\Omega} \rightarrow \dfrac{watts}{sr \bullet cm^2}$

Usually the above relations are dependent on the wavelength, and a 1/μm factor could appear multiplying those units, which then represent "spectral" quantities.

If $\delta A$ is part of a "point source", then the radiant flux will be independent of the direction.

If $\delta A$ is part of an extended Lambertian source, then the radiant flux will not be distributed uniformly with direction as shown in Figure 3. 2, and the following relation will be true: $\delta\phi_\theta = \delta\phi_n \bullet \cos\theta$

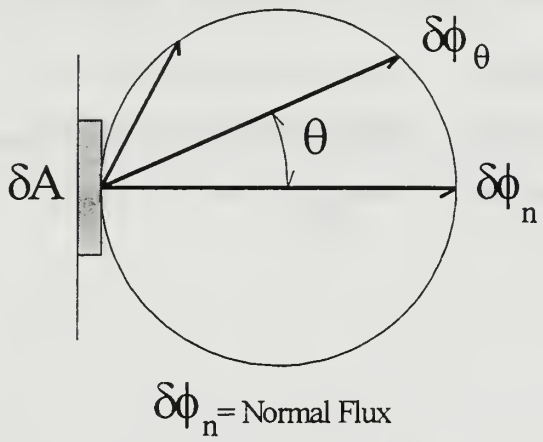


Figure 3. 2 Radiant Flux in a Lambertian Extended Source.

Then, for a Lambertian source: $L_\theta = \dfrac{(\delta\phi_\theta)^2}{\delta A \bullet \cos\theta \bullet \delta\Omega} = \dfrac{(\delta\phi_n)^2}{\delta A \bullet \delta\Omega} = constant$, and the radiance is independent of the observing direction.

## B. RADIATION INTERACTION

For targets located in the sea, the radiation that goes into the sensor can be represented as depicted in Figure 3. 3, where the specularly reflected sun component refers to the sun radiation reflected from the sea and "τ" refers to transmittance. The use of Figure 3. 3, Figure 3. 4, and Figure 3. 5 will allow us to write the total energy that goes into the sensor and therefore to predict the temperature.

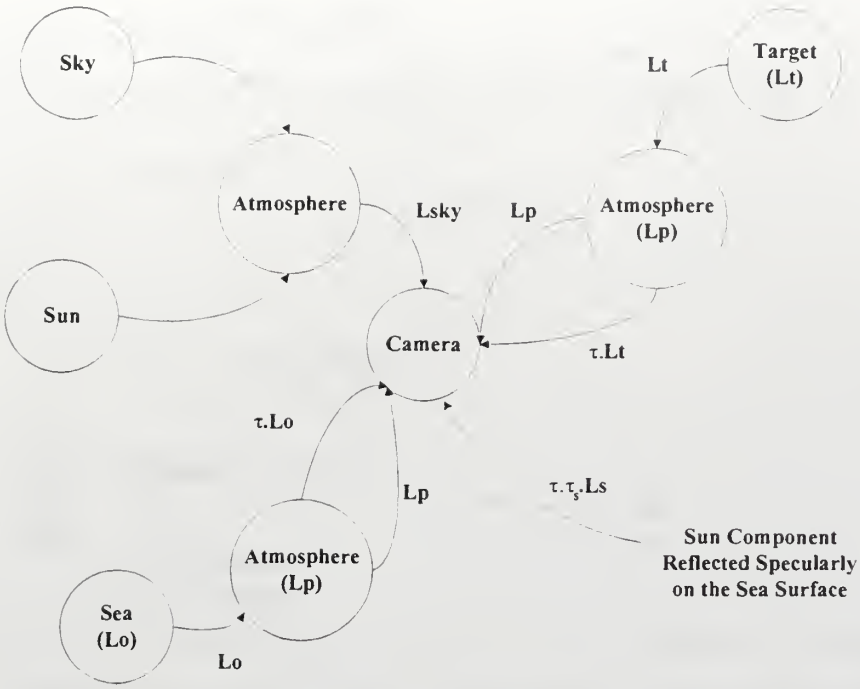


Figure 3. 3 Sources of Radiation for the EOPACE Data.

The sun depicted in Figure 3. 3 is not in the field of view (FOV) of the sensor. However, it acts indirectly, exchanging energy with the atmosphere constituents visible to the camera FOV.

Note that the atmosphere, the scattering of the sun on the atmosphere and the sky represent the same entity, but here they were separated didactically in order to identify clearly the atmospheric irradiance involving a specific path, the source irradiance and the atmospheric attenuation.

In order to see more clearly the interaction of the radiation, it is worthwhile to depict what is incident on the target (Figure 3. 4) and on the sea (Figure 3. 5).

In these levels of presentation, no information was added regarding the dependence of radiance on geometric and other variables such as temperature and wavelength. But those variables have a great impact on the values of the radiance and should also be considered.

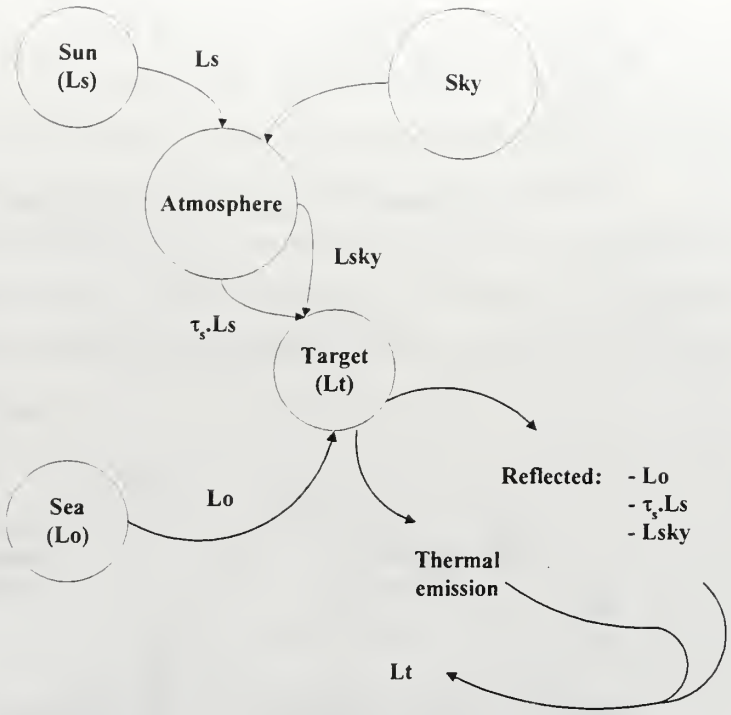


Figure 3. 4 Radiation Hitting the Target: Sources and Attenuation.

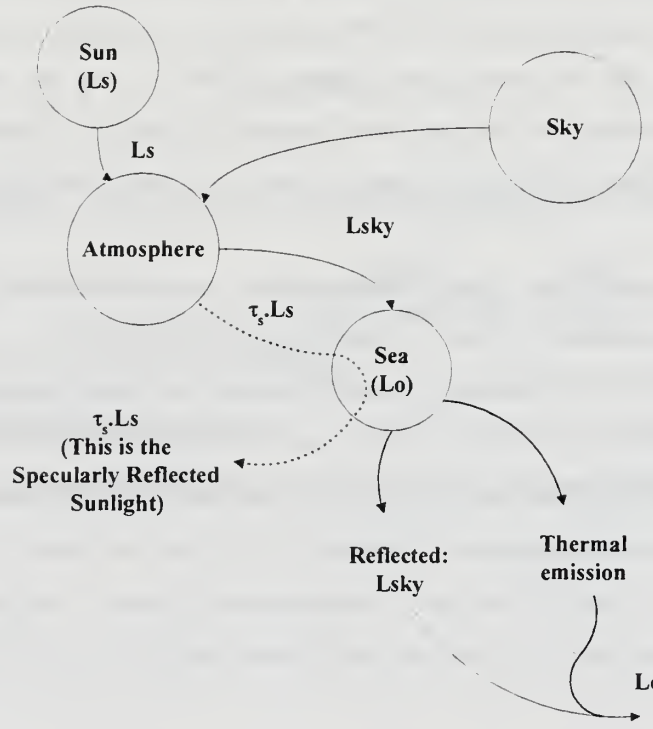


Figure 3. 5 Radiation Hitting the Sea: Sources and Attenuation.

## C. TEMPERATURE DEFINITION

Planck's law relates black body irradiance to temperature and wavelength.:

$$M(\lambda) = \frac{C_1}{\lambda^5} \bullet \frac{1}{e^{\frac{C_2}{\lambda \bullet T}} - 1} \tag{3.1}$$

Where:

- $C_1 = 3.7415 \ \ 10^4 \ \frac{watts \bullet \mu m^4}{cm^2}$
- $C_2 = 1.4388 \ \ 10^4 \ \mu m \bullet K$
- $M$ in $\frac{watts}{cm^2 \bullet \mu m}$

Then, the apparent temperature of an object ($T_r$) is, by definition, the corresponding temperature of a black body, that would radiate the same amount of energy as that radiated by the object [Ref. 2].

$$[\Sigma M(\lambda)]_{object} = [\Sigma M(\lambda)]_{(Black\ Body\ at\ Temperature\ T_r)} \tag{3.2}$$

Applying the Planck law:

$$[\Sigma M(\lambda)]_{object} = \int_{\lambda 1}^{\lambda 2} \frac{C_1}{\lambda^5} \bullet \frac{1}{e^{\frac{C_2}{\lambda \bullet T_r}} - 1} \bullet d\lambda \tag{3.3}$$

For opaque objects the expression for the radiant exitance can be written as the sum of its thermally emitted exitance plus the reflected exitance components of radiation ($R$) from different sources, thus:

$$[\Sigma M(\lambda)]_{object} = \int_{\lambda 1}^{\lambda 2} \left( \frac{C_1}{\lambda^5} \bullet \frac{\varepsilon}{e^{\frac{C_2}{\lambda \bullet T_O}} - 1} + R \right) \bullet d\lambda \tag{3.4}$$

Where:

- $\varepsilon$ is the emissivity.
- $T_O$ is the object temperature.
- $R$ is the reflected exitance.

It should be clear that the radiant exitance of the object will be attenuated by the atmosphere and it will combine with other exitances (Figure 3. 3) before it reaches the sensor. Hence, the final expression will be very complex, and some simplification will be required to solve it.

### 1. Ship Radiant Exitance

Considering the ship as the object and considering it as an extended Lambertian source, then:

$$M = \pi \bullet L \tag{3. 5}$$

This assumption can be made because the ship image appears to have a flat and uniform radiance distribution and in consequence, using Figure 3. 4:

$$R = \pi \bullet \left(\rho_{t,o} \bullet L_o + \rho_{t,s} \bullet \tau_s \bullet L_s + \rho_{t,sky} \bullet L_{sky}\right) \tag{3. 6}$$

In the above equation $\rho_{t,o}$, $\rho_{t,s}$ and $\rho_{t,sky}$ each represents the reflectivity of the ship for the radiation from the sea, sun and sky respectively. It is a function of the direction of incidence of radiation on the target and the wavelength.

Using Figure 3. 5, the sea radiance "$L_o$" can be expanded one level more.

$$Lo = Lsea + Lrsky + Ls \tag{3. 7}$$

Where:

- *Lsea* is the sea emission.
- *Lrsky* is the reflected sky radiance.

Shumaker [Ref. 2] wrote that most military targets approximate gray bodies in the 8-12 μm band with emissivities of the order of 0.9 to 0.95 in that spectral region. The emissivity of the R/V POINT SUR has been reported as 0.95 in a private communication (A. W. Cooper), and in consequence is in accordance with Shumaker.

For an opaque target in thermal equilibrium the emissivity and the reflectivity are related by:

$$\varepsilon + \rho = 1 \tag{3. 8}$$

Thus high emissivity means low reflectivity, the value of "R" in Equation 3.4 will be small and the major contribution to irradiance from the ship will come from its emission. Hence, the target reflectivity will be constant and the maximum error that will result from this assumption will have the magnitude of the reflectivity.

$$\rho_t = \rho_{t,o} = \rho_{t,s} = \rho_{t,sky} = 0.05 \tag{3.9}$$

$$R = \pi \bullet \rho_t \bullet \left(L_o + \tau_s \bullet L_s + L_{sky}\right) \tag{3.10}$$

**2. Sea Radiant Exitance**

If the object were a source other than the ship, the "R" expression would change. Assuming again that the sea is a Lambertian source and using Figure 3. 5:

$$R = \pi \bullet \left(\rho_o \bullet L_{sky} + \tau_s \bullet L_s\right) \tag{3.11}$$

For the sea, any energy transmitted through the surface is considered absorbed (except perhaps in very shallow waters) and therefore we may write:

$$\varepsilon + \rho = 1 \tag{3.12}$$

Of those backgrounds considered in Figure 3. 3, the sea is the hardest to solve for the complicated geometry of reflection due to the randomness of wavelets and its significant relationship with atmospheric conditions, mainly the wind direction and intensity. But, it has been studied extensively, and the SeaRad program can be used to help in computing the exitance contribution from the sea.

The sea emissivity is a function of the wavelength and the radiation incident angle. But from [Ref. 2], the use of the average emissivity introduces an error less than 2% for the 4-10 μm band.

The sea emissivity does not depend on the sun position but it has a large dependency on wind intensity and direction and on the weather conditions.

**3. Sky Vault Radiant Exitance**

From [Ref. 11], the radiance of the sky is the sum of the emission by the atmospheric constituents and the scattering of the sun's radiation. Molecular scattering is important only in the short-wave region neighboring the visible, and the emission is important for wavelengths longer than 4 μm.

Note that the reflectivity concept is now replaced by the scattering concept, which is more convenient to deal with for the aerosol and molecular atmosphere components. SeaRad does not make any distinction between the emission and the scattering radiance, and refers to the sum of the two radiances as "path radiance".

#### 4. Atmospheric Radiant Exitance

Here, the same considerations from the previous Sub-subsection 3 will be applied, but now, the path considered is the one that contains the air mass between the sensor and the object under study instead the one between the sky and the sensor.

#### 5. Sun Radiant Exitance

The sun radiation will heat the atmospheric constituents, adding a contribution to the atmosphere emission, and also will generate three kind of radiances: the scattered sun radiance, the sun radiance specularly reflected from the sea surface, and the sunlight scattered by particles beneath the sea surface. The latter, [Ref. 9], is nearly independent of the presence of waves and can be neglected for large distances from the observer.

The scattering is a complex phenomenon that involves atmospheric constituents, optical and solar path, sun position and the model of scattering: single or multiple. In [Ref. 5], the authors claim that a single scattering model is good only when looking near the sun, since the scattering then is dominated by forward peaks.

The sun radiation reflected from the sea surface is also very complex since one of its variables is the wavelet geometry, which is a random variable.

Fortunately, there is a program named Sea Radiance Prediction Code (SeaRad) that manipulates those complexities, and there is no need to worry about the "R" expression for the reflected sun radiation on the sea surface.

# IV. INPUT PREPARATION

This chapter will present the available data and some data manipulation that will make them ready to be used as the input for the range compensation method.

The core of the work is based on the utilization of SeaRad either to justify a point of view or to get new data.

To obtain the sun coordinates a shareware version of the Cybersky 3.0.2 software was used. For mathematical calculations or image processing Mathcad or Matlab in combination with the PTRWIN software was used.

## A. BASIC INPUTS

The basic inputs are those that define the problem. The file "NSD1003.ptw" was chosen as a model for calculation of range compensation because it shows the ideal image conditions for this analysis. The target is in the center of the picture, the target contour is well defined (good contrast), and the horizon line is sharply defined.

The main data list and its origins are listed below.

From [Ref.8]:

- Observer latitude: 32° 39' 55" = 32.6653°.
- Observer longitude: 117° 14' 31" = 117.2419°.

From [Ref. 7]:

- Observer height: 27.4 meters.

From the image file "NSD1003.ptw":

- Date: April 10, 1996.
- (Hour:minutes:seconds): 10:27:28 AM PST ≡ 17:27:28 GMT
- $\Delta w = (176 - 152) = 24$ lines (see Figure 2. 15).
- $w = 256$ lines.

From the meteorological file "eop30sec.101":

- Wind speed: 1 m/s.
- Wind direction: 238°.
- Air temperature: 16.4 °C.
- Relative humidity: 73%.
- Air pressure: 1,016.2 mbar.

- Sea surface temperature: 17.6 °C.
- Ship latitude: 32° 39' 6" = 32.6517°.
- Ship longitude: 117° 13' 42" = 117.2283°.

From Cybersky:

- Sun altitude: 48° 58' 8" = 48.969°.
- Sun azimuth: 118° 29' 54" = 118.498°.

From calculation, using Equation 4.1 through Equation 4.6:

- Target distance from observer: 1,980.7 meters.
- Target Bearing: 139.91° East from North.

For the determination of the target range and bearing the following equations were used:

$$A = \psi - \psi_o \tag{4. 1}$$

$$b = \frac{\pi}{2} - \mu_o \tag{4. 2}$$

$$c = \frac{\pi}{2} - \mu \tag{4. 3}$$

$$a = cos^{-1}(cos\, b \bullet cos\, c + sin\, b \bullet sin\, c \bullet cos\, A) \tag{4. 4}$$

$$range = re \bullet a \tag{4. 5}$$

$$bearing = sin^{-1}\left(\frac{cos\, \mu \bullet sin(\psi - \psi_o)}{sin\, a}\right) \tag{4. 6}$$

Here *re* is the radius of earth, the observer position is $(\mu_o, \psi_o)$, specified in latitude and longitude, the target position is $(\mu, \psi)$, also in latitude and longitude, and the bearing is measured taking the North Pole direction as the reference position.

From Equation 2.13 and using the 7° lens, $x_T$ = 1,917 meters. This shows that:

- FOV used for this image is 7°.

From experiment notebook:

- Weather: overcast with cloud and 3,500 feet scatter. Thus, the weather input is ICLD = 2: Altostratus cloud with base 2.4 km.

The geometry of the experiment for this particular case is shown in Figure 4. 1.

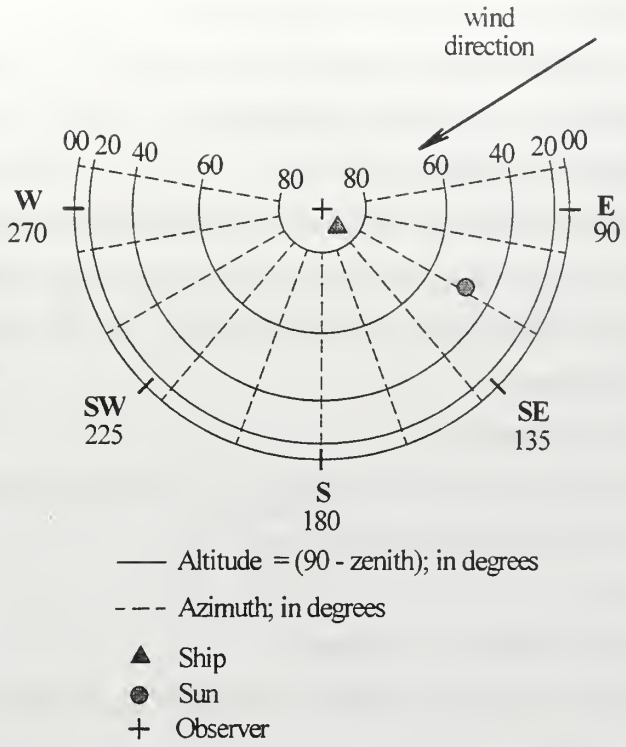


Figure 4. 1 The Geometry for the File "NSD1003.ptw" Case.

Note from Figure 4. 1 that the Sun is in a good position for glint formation, but unfortunately the wind intensity is very low. Thus, the wind does not favor high values of Sun glint. However, the main limitation for setting up the Sun glint is the overcast condition on the experiment date.

## B. BASIC CONSIDERATIONS

### 1. SeaRad Input File

SeaRad uses "Tape5" as its input and the format is nearly the same as its predecessors LOWTRAN and MODTRAN. The variation is mainly in the additions that SeaRad made in computing sea radiance.

In this thesis the following basic instructions for SeaRad will be used:

- Run option: MODTRAN.
- Atmospheric model: Midlatitude Summer.
- Atmospheric path: Vertical or slant path to space.
- Program execution in radiance mode with solar scattered radiation.

- Program executed with multiple scattering.
- Use of U.S. Standard altitude profile.
- Boundary temperature: Sea temperature.
- Surface albedo (ocean): -5.
- Type of extinction for boundary layer: Navy Maritime extinction.
- Seasonal aerosol profile for boundary layer: Spring-Summer.
- Type of extinction and aerosol profile for stratospheric-layer: Background stratospheric.
- Air mass character: 3.
- No use of the Army Vertical Structure Algorithm for aerosol boundary layer.
- Use of default meteorological range.
- No rain.
- Observer altitude: 27.4 meters.
- MIE-generated SeaRad internal database of aerosol phase functions.

**2. Sea Emission**

Because the sea is the main background in the EOPACE experiment, most range compensation will happen on the sea image. Thus, it is required to find the sea radiance behavior as a function of the incident angle (zenith angle of the observer; seen from the footprint). Using SeaRad the data of Table 4. 1 can be found for the file "NSD1003.ptw" boundary conditions.

| Incident Angle | Sea Emission (watts/m$^2$/sr) | Average Sea Emissivity | Sky Reflection (watts/m$^2$/sr) | Sun Glint watts/m$^2$/sr | Total Irradiance (watts/m$^2$/sr) | Sea Temperature |
|---|---|---|---|---|---|---|
| 89.8 | 14.1688 | 0.4234 | 19.6022 | 0 | 33.77101 | 18.3 |
| 89.6 | 14.2474 | 0.4258 | 19.5397 | 0 | 33.78710 | 18.4 |
| 89 | 14.7160 | 0.4398 | 19.0787 | 0 | 33.79477 | 18.4 |
| 87 | 16.7215 | 0.4999 | 15.8091 | 0 | 32.53063 | 16.2 |
| 85 | 18.8140 | 0.5625 | 13.8947 | 0 | 32.70872 | 16.5 |
| 83 | 20.8576 | 0.6237 | 11.7054 | 0 | 32.56299 | 16.2 |
| 80 | 23.6995 | 0.7090 | 9.35541 | 0 | 33.05492 | 17.1 |
| 75 | 27.3751 | 0.8194 | 5.87379 | 0 | 33.24892 | 17.5 |
| 70 | 29.68692 | 0.8890 | 3.60931 | 0 | 33.29623 | 17.5 |
| 65 | 31.05535 | 0.9304 | 2.23421 | 0 | 33.28956 | 17.5 |
| 60 | 31.85211 | 0.9546 | 1.43539 | 0 | 33.28750 | 17.5 |
| 50 | 32.58303 | 0.9769 | 0.71274 | 0 | 33.29577 | 17.5 |

Table 4. 1 Sea Radiance Data for File "NSD1003.ptw".

To get a feeling for the influence of weather on the reflectivity, that is (1 - emissivity), and to compare with other authors' curves, the plot of Figure 4. 2 was built. Unfortunately the authors of [Ref.2] and [Ref. 6] did not specify the weather conditions. However, from Figure 4. 2 and considering the magnitude of the results, it is clear that both authors considered the "no clouds" condition.

Notice the effect of wind on the reflectivity: as the reflectivity increases the wind intensity also increases.

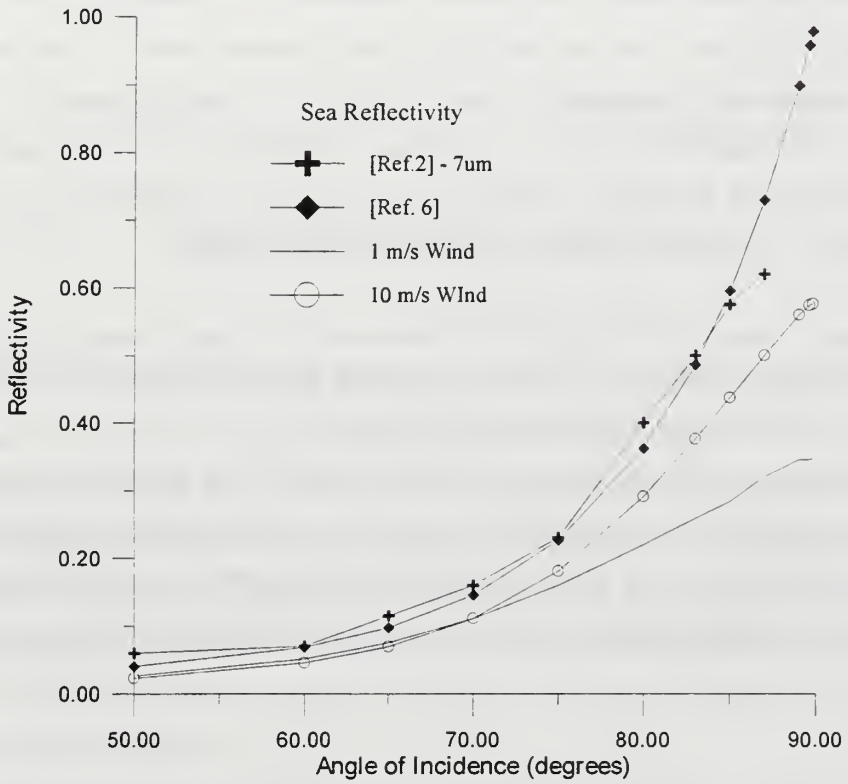


Figure 4. 2 Comparison of Reflectivity.

Using polynomial fitting, the sea reflectivity "$\rho_o$" for 1 meter/sec wind speed of this file can be written as a function of the angle of incidence "$a$" in degrees as:

$$\rho_o(a) = D6 \bullet a^6 + D5 \bullet a^5 + D4 \bullet a^4 + D3 \bullet a^3 + D2 \bullet a^2 + D1 \bullet a^1 + D0 \qquad (4.7)$$

Where:

- D0: -74.9072
- D1: 6.97542

- D2: -0.269547
- D3: 0.00553385
- D4: -6.36474E-005
- D5: 3.88588E-007
- D6: -9.81879E-010

This formulation will be used in Chapter 5 for correction of the SeaRad sky reflection.

### 3. Picture Geometry

One important factor in atmospheric attenuation is the distance. Thus, it is necessary to determine all the points in the picture that have equal distances relative to the observer.

Considering a plane earth with plane equation: $z = 0$, and the observer positioned at the rectangular coordinate $(0, 0, h)$, then the locus of all points on the earth equidistant from the observer will be the intersection of the sphere of radius $re$ (all points in the space that have the same distance to the observer) and the earth, which can be written:

$$x^2 + y^2 = re^2 - h^2 \tag{4. 8}$$

This shows that the observer will perceive the points having the same distance from him as lying on a circle. The geometry is consistent with Figure 2. 14.

Assuming that the nearest target picture will be at 1 km and that the target is in center of the picture, then the nearest point in the picture will be at approximately 308.83 meters from the observer (see Figure 4. 3. b). Even for this small distance the points at the same distance to the observer can be approximated as lying on a horizontal line with at worst an error of 0.58 meters.

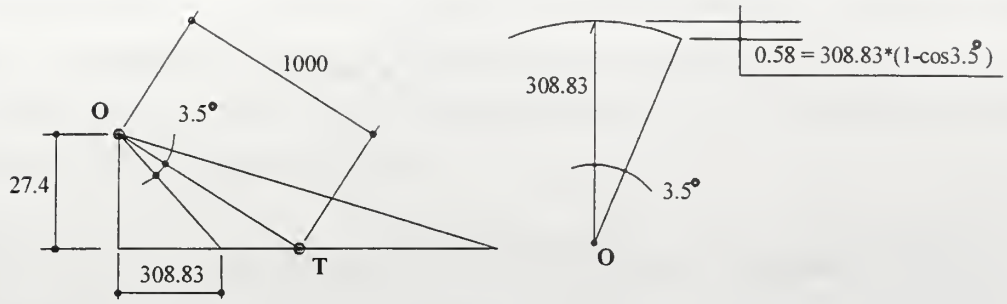


a) Elevation View

a) Plan View. 3.5° is the azimuthal angular width of the scene

Figure 4. 3 Picture Geometry: General Case.

This fact is very favorable for the solution of this thesis since in order to make a picture compensation all that is necessary is to know the atmospheric parameters as a function of distance for just one particular azimuth direction, specifically, the target direction.

The ship itself should be considered differently from the sea because all points located on the ship can be considered to have the same distance to the observer. That fact will be beneficial because the ship contrast will be improved when using the range compensation method where the sea surface background approaches the horizon (the background temperature will decrease).

For figuring out the incident angles of interest for the file "NSD003.ptw", Equation 2.10 can be used to build up Figure 4. 4.

The target-horizon distance in image coordinates is: $\Delta w = (176 - 152) = 24$ pixels. The distance from the lowest point on the image plane to the horizon is: $\Delta w = (256 - 152) = 104$ pixels. The target position considered was location 3 of Figure 2. 16, that is "water aft" probe position.

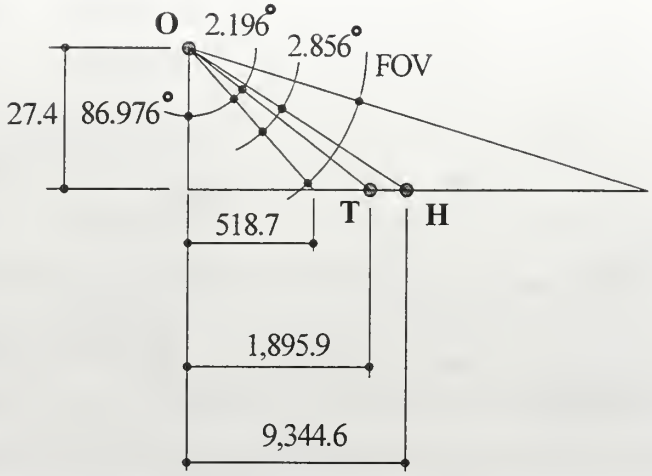


Figure 4. 4 Picture Geometry in Vertical Plane for File "NSD1003.ptw".

Considering that the zenith angle of the observer line-of-sight is 180° minus the incident angle, for the sea compensation this angle will vary from 93.02° to 90.168° and for sky from 90.168° to 86.02°. The horizon zenith angle of 90.168° is only an approximate value. The correct horizon zenith angle can be determined by plotting the sky path radiance versus observer zenith angle, as will be done later in Subsection 5.

**4. Target Temperature**

The target itself is the main component in the thermal image picture. Therefore, it is desirable to check the quality of the ship temperature distribution recorded with the AGA, Figure 4. 5, by comparing it with the skin temperature recorded with the thermistors, shown in Figure 4. 6.

In fact, it is impossible to associate quantitatively each channel position with its corresponding point in the picture due to the following facts:

- The ship is not perfectly transverse to the target line-of-sight.
- The position coordinates of the thermistor are very loosely specified.
- The exchange of thermal energy between the ship and the surroundings produces temperature perturbations around the ship. Thus the exact ship profile cannot be determined from the image.

Nevertheless, qualitatively the data seem to be correct, with a region of high temperature near the port stack, another region with low temperature that follows the ship profile and finally

the surrounding sea temperature. The comparison should also be considered qualitative because the AGA temperature is an apparent temperature that incorporates the path radiance, atmospheric radiance, radiance reflected by the target, and the target emission radiance. On the other hand, the thermistor temperature considers only the target emission temperature.

Table 4. 2 can be built for these three regions, where the 2.3± 1.7 °C added to the AGA temperature refers to the calibration correction.

| Region | AGA Temperature (°C) | Thermistor Temperature (°C) |
|---|---|---|
| Port Stack | 20 + (2.3± 1.7) | 26.8 |
| Ship Contour | (13 to 14) + (2.3± 1.7) | 16.3 |
| Sea Near Ship | 12 + (2.3± 1.7) | 14.5 |

Table 4. 2 Qualitative Comparison of Temperature: Corrected Radiometric Temperature Versus Thermistor Temperature.

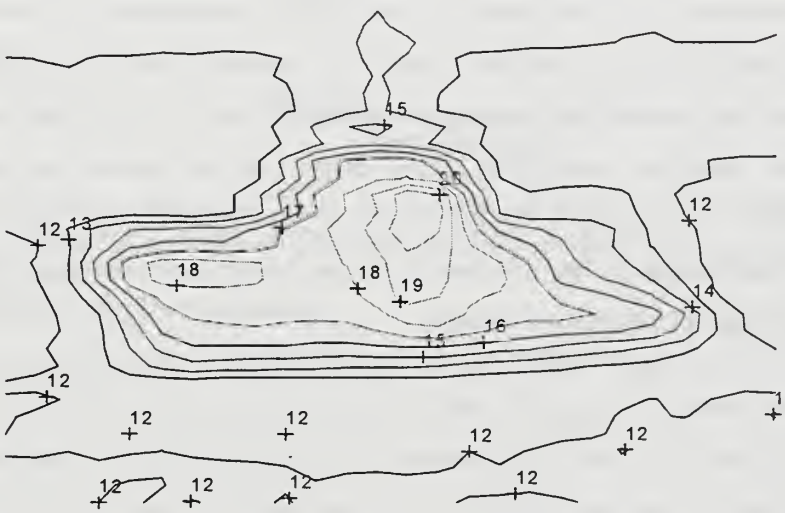


Figure 4. 5 Thermal Image Temperature Distribution Uncorrected for Path Radiance.

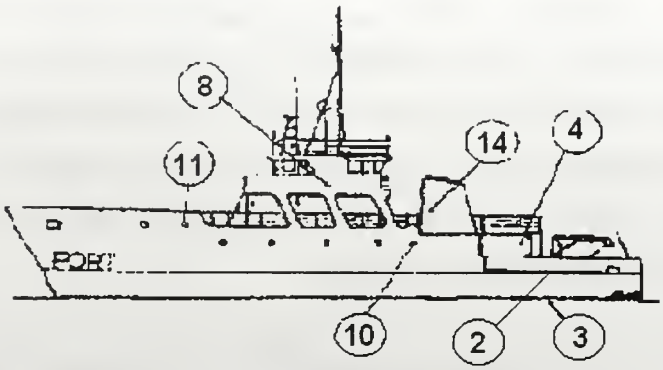


Skin Temperature: April 6, 1996
10:27:28 AM PST

| | | | |
|---|---|---|---|
| 11-16.386 | 8-16.754 | 14-26.857 | 4-16.401 |
| | | 10-17.267 | 2-16.918 |
| | | | 3-14.572 |

Figure 4. 6 Thermistor Temperature: Temperatures Recorded by Selected Thermistors in File "eop30sec.101".

Note that in file "eop30sec.101" the METOC measurement of sea surface temperature is 17.6 °C, whereas the skin thermistor number 3 recorded a sea surface temperature of 14.5 °C. Comparing these outputs as time series as shown in Figure 4. 7, it is clear that the METOC value follows the thermistor value with a time delay. Several reasons can be advanced for such differences.

The influence of this difference in the sea temperature will be analyzed better later in the following Range Compensation Chapter.

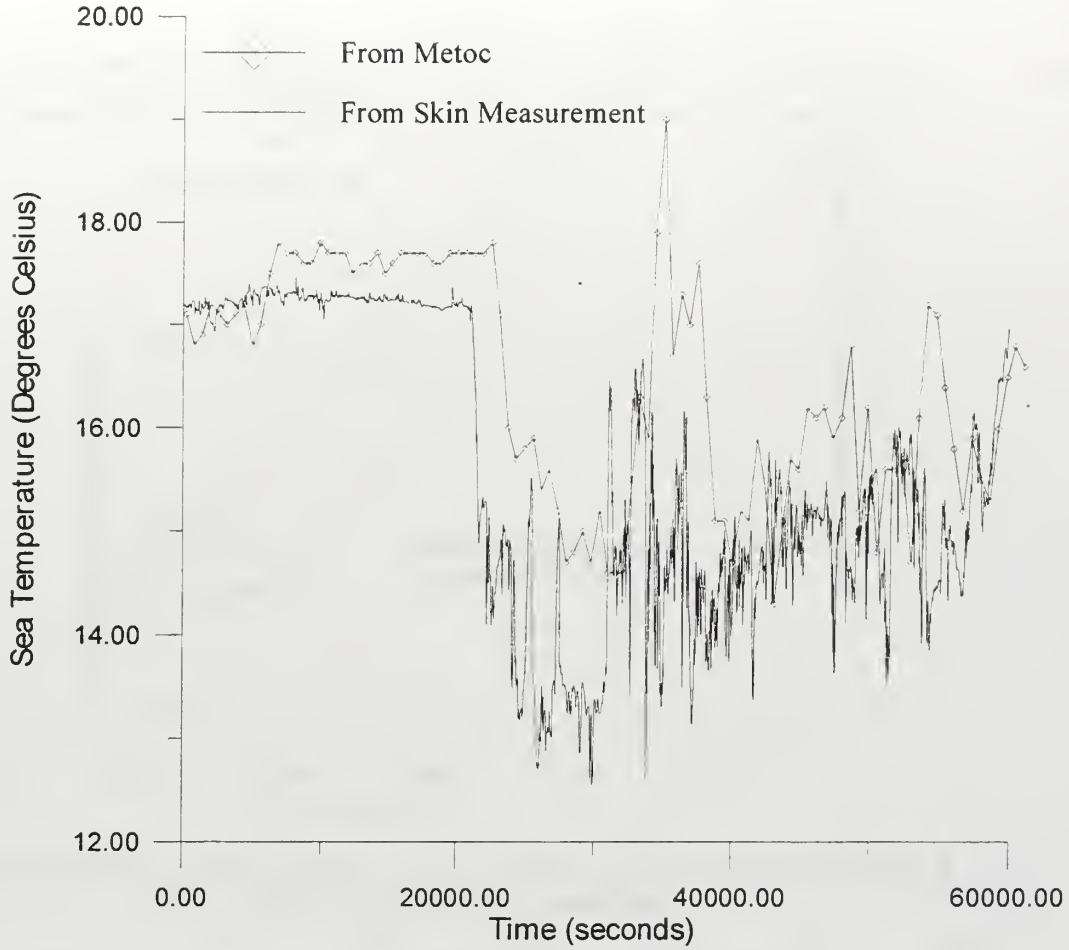


Figure 4. 7 Comparing Temperature Data: Sea Surface Temperature from Thermistor 3 Compared with R/V POINT SUR METOC Measurement.

### 5. The Horizon Determination

The correct identification of the horizon position is needed since the sky path radiance has a pattern completely different from the sea path radiance. Figure 4. 8 shows computed path radiance versus frequency with zenith angle as a parameter. We see that at any frequency the path radiance rises as the horizon is approached from either direction, with a sharp maximum at the horizon. This condition is represented by the dotted line for 90.15°, identifying the optical horizon.

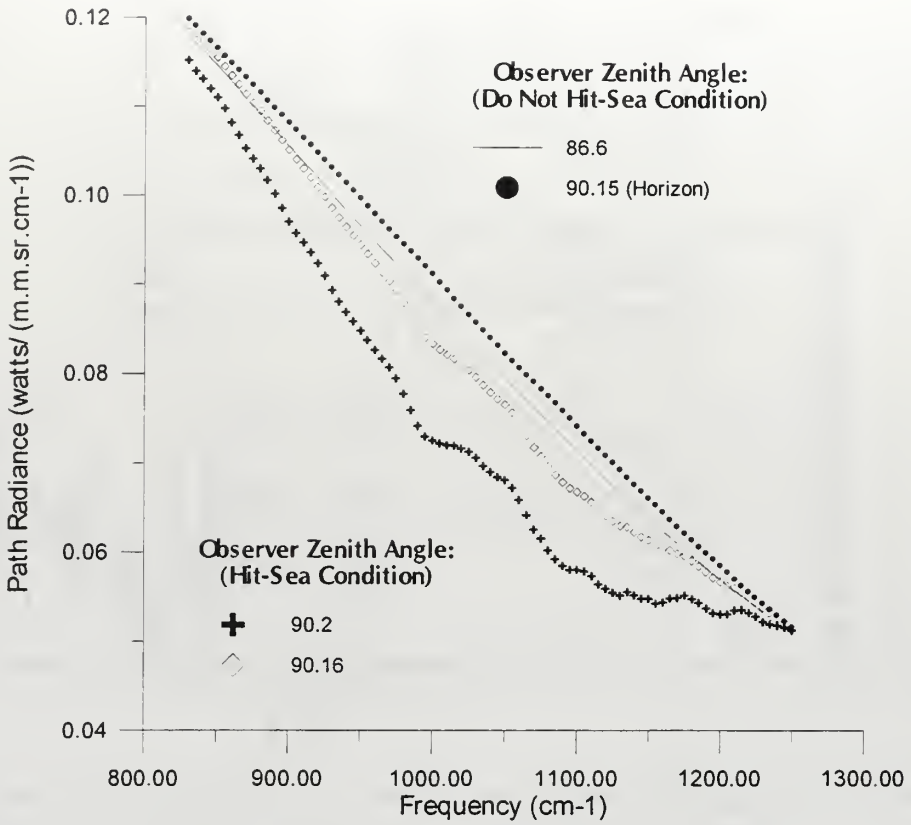


Figure 4. 8 Path Radiance for Different Zenith Angles. The Maximum Path Radiance at 90.15° is Indicative of the Optical Horizon.

Running SeaRad for other observer zenith angles and integrating the path radiance versus frequency curve, Table 4. 3 can be built for varying zenith angles.

| Zenith Angle (degree) | Path Radiance watts/($m^2$.sr) |
|---|---|
| 78.25 | 33.4 |
| 86.60 | 34.5 |
| 88.50 | 35.01 |
| 89.00 | 35.2 |
| 90.00 | 35.4 |
| 90.15 | 35.6 |
| 90.16 | 33.7 |
| 90.20 | 30.7 |
| 90.60 | 17.2 |
| 90.80 | 14.3 |

Table 4. 3 Spectrally Integrated Path Radiance as a function of Zenith Angle

Plotting the data of Table 4. 3 will provide a better view of the horizon position as long as the path radiance of the sea is much smaller than the sky path radiance (see Figure 4. 9).

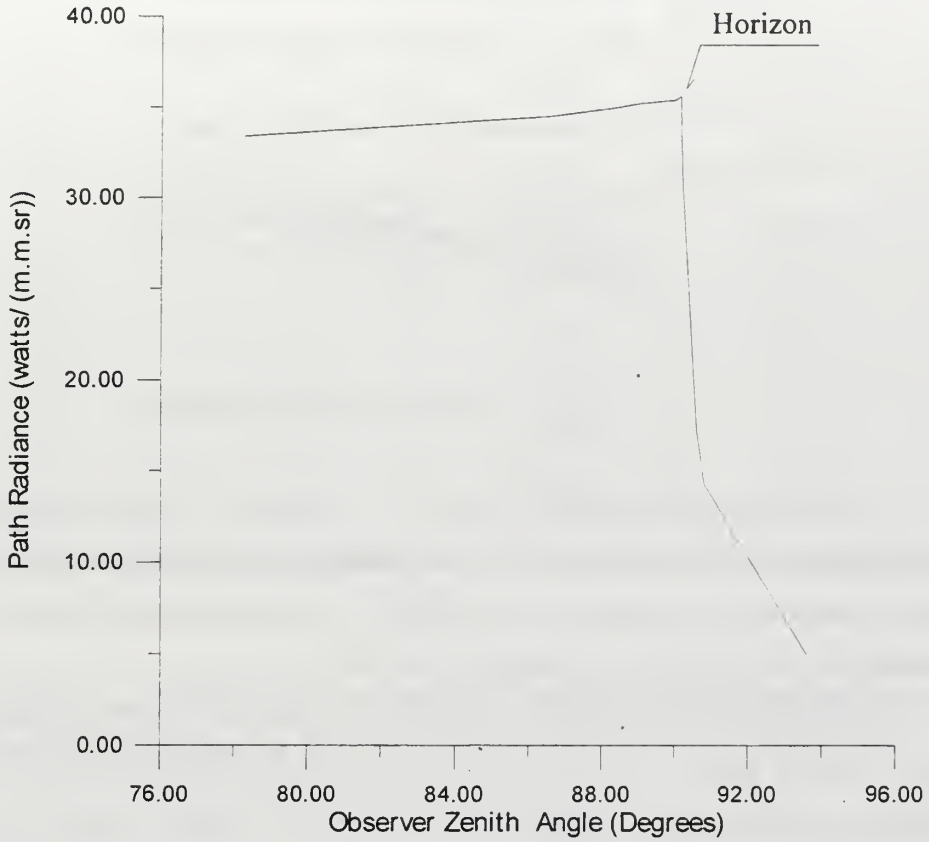


Figure 4. 9 The Horizon Determination. The Sharp Discontinuity in Radiance Identifies the Horizon.

Finally, from Figure 4. 9, the observer will see the horizon at a zenith angle of 90.15°. This horizon zenith angle takes into account the ray bending and the spherical earth. Using plane earth calculations 90.168° was found instead of 90.15° (see Figure 4. 4). This shows the validity of using plane earth geometry.

In terms of temperature, the sky path radiance can be seen better in the isotherm display mode as in Figure 4. 10, where the calibration correction has not been applied yet. Note that unlike the sea the sky does not have random sources of radiance such as the ones seen in the lower left of the image, unless broken clouds and sun glitter are present.


Figure 4. 10 Uncorrected Sky Isotherms.

According to MacCartney, [Ref. 3], the calculation of the sky radiance imposes two difficulties: the sky does not have area and, principally, the sky does not have definite distance from the observer. This means that the concept of range compensation loses its meaning when it is applied to the sky because the distance is indefinite.

For that reason, the range compensation will apply only for the sea and the ship with the observer zenith angle varying from 93.02° to 90.15° for this particular file "NSD1003.ptw". However, the sky radiance will not be overlooked and will play a major role in tuning up the SeaRad sky radiance by adjusting the sky path radiance and comparing the SeaRad output with the temperature of Figure 4. 10.

To determine the sensitivity of path radiance to the major parameters used in SeaRad, the comparative Table 4. 4 was constructed from multiple SeaRad runs with varied values of Air Mass Character (ICSTL), Cloud and Rain Model (ICLD) and Surface Meteorological Range. The calculated results show that changes in ICSTL and in Surface Meteorological Range produce insignificant variation in the path radiance over the range of parameters used.

| ICSTL (The Air Mass Character) | ICLD (Clouds and Rain Model ) | Surface Meteorological Range (Km) | Total Lpath (watts/$m^2$/sr) |
|---|---|---|---|
| 1 | 0 | default | 35.56 |
| 5 | 0 | default | 35.58 |
| 9 | 0 | default | 35.62 |
| 3 | 0 | default | 35.58 |
| 3 | 5 | default | 63.08 |
| 3 | 9 | default | 55.40 |
| 1 | 0 | 100 | 36.60 |
| 1 | 0 | 1000 | 35.32 |
| 1 | 0 | 10,000 | 35.32 |

Table 4. 4 Influence of Meteorological Parameters on Path Radiance for the Horizon Zenith Angle.

From Table 4. 4, it can be seen that there is a lower limit for the path radiance below which the sky path radiance cannot be decreased.

This Page Intentionally Left Blank

# V. RANGE COMPENSATION

This chapter will present a step by step procedure for the range compensation method for the file "NSD1003.ptw". As stated in the previous chapter, the range compensation will be applied only for the sea and the ship, with the observer zenith angle varying from 93.02° to 90.15°.

## A. DATA MANIPULATION

The range compensation process is not an easy task and the complexity can be appreciated with the help of the picture of Figure 5. 1. For each specific distance the observer measures an apparent black body temperature of *Tapp-FR*. This temperature corresponds to an irradiance *Ms* (area under the black body irradiance curve) that allows the calculation of the zero range irradiance *Mo*, knowing the atmospheric transmittance and the path radiance. The range compensation then ends for that distance by computing the apparent black body temperature at zero range, *Tapp-ZR*, which corresponds to *Mo*.

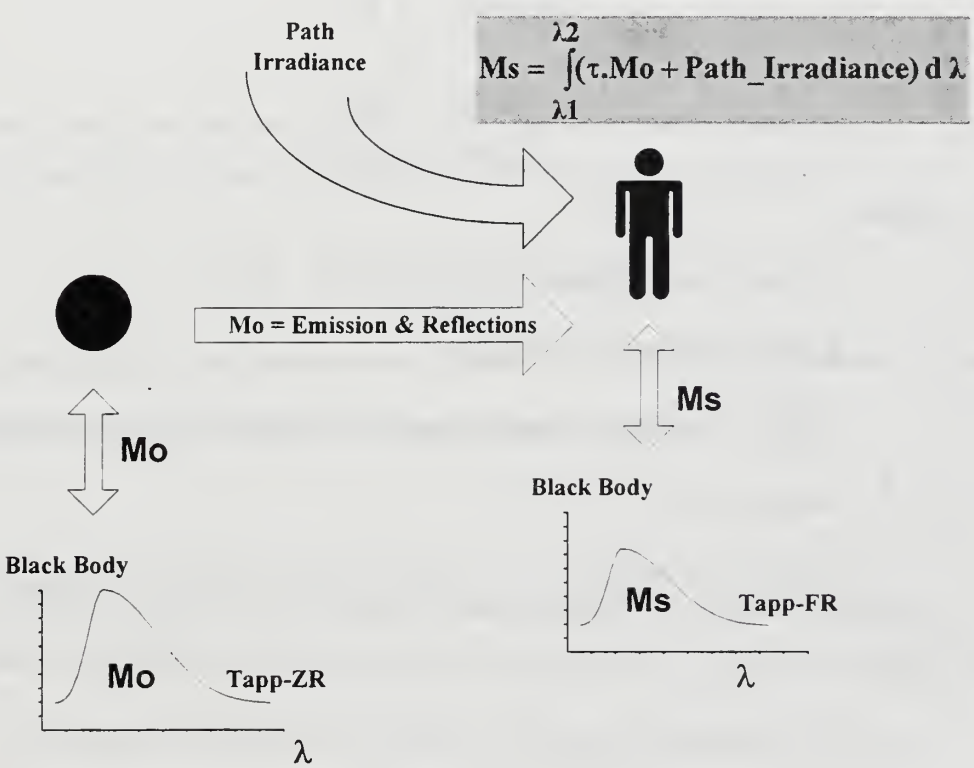


Figure 5. 1 The Range Compensation Problem.

Note that the above process is very extensive because it should be applied over all pixels of the image plane and in consequence a better algorithm should be found.

The first step in that direction is to define the tools that will be used: matrix variables. In order to manipulate the wavelength dependency for the infrared radiation parameters, first, the smallest frequency step size allowed by MODTRAN (5 $cm^{-1}$) needs to be selected. Then, all SeaRad output should be standardized to vary over the same frequency bandwidth of 830 $cm^{-1}$ to 1250 $cm^{-1}$, with a total of 85 frequency points in this range. That is:

$$\bar{\nu} = \begin{bmatrix} 830 \\ 835 \\ \vdots \\ 1245 \\ 1250 \end{bmatrix} = \begin{bmatrix} \nu_1 \\ \nu_2 \\ \vdots \\ \nu_{84} \\ \nu_{85} \end{bmatrix} \tag{5. 1}$$

$$\bar{\lambda} = \frac{10{,}000}{\bar{\nu}} = \begin{bmatrix} 12.048 \\ 11.976 \\ \vdots \\ 8.032 \\ 8.000 \end{bmatrix} = \begin{bmatrix} \lambda_1 \\ \lambda_2 \\ \vdots \\ \lambda_{84} \\ \lambda_{85} \end{bmatrix} \tag{5. 2}$$

Where:

- $\bar{\nu}$ is the constant frequency vector in $cm^{-1}$.
- $\bar{\lambda}$ is the wavelength vector in $\mu m$.
- $\frac{10{,}000}{\bar{\nu}}$ represents a Matlab operation of scalar division by elements of the frequency vector.

The result of this standardization is that the SeaRad output can now be manipulated as a matrix, as shown in Figure 5. 2, where each of its columns shows a frequency dependence.

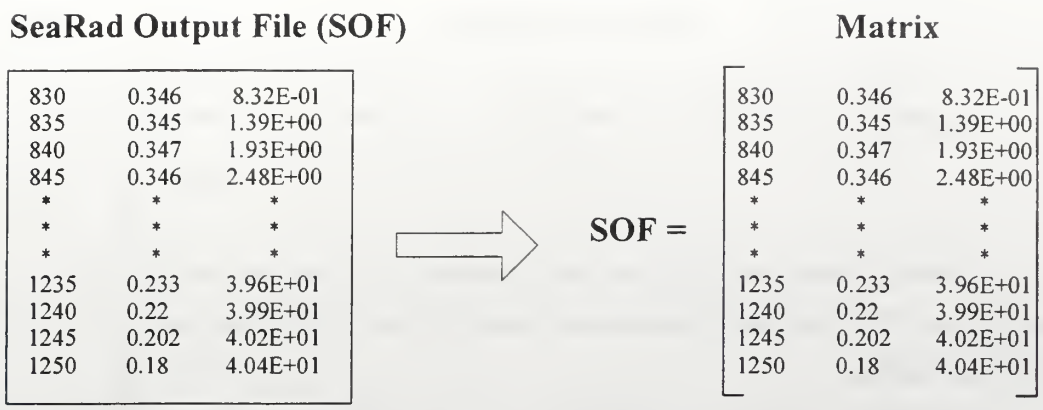


Figure 5. 2 Transformation of Text File into Matrix Variable.

For example, if the third column represents the path radiance, then it can be written:

$$Lpath(\nu) = SOF(*,3) = \begin{bmatrix} Lpath(\nu_1) \\ Lpath(\nu_2) \\ \vdots \\ Lpath(\nu_{84}) \\ Lpath(\nu_{85}) \end{bmatrix} = \begin{bmatrix} 8.32E-01 \\ 1.39E+00 \\ \vdots \\ 4.02E+01 \\ 4.04E+01 \end{bmatrix} \tag{5.3}$$

Accordingly, all data manipulations will be treated as matrix operations.

Frequently the average value is needed. Its integral form is as follows:

$$average \quad of \quad f(\nu) = \frac{1}{b-a} \bullet \int_a^b f(\nu) d\nu \tag{5.4}$$

Taking again the path radiance as an example, we will have for the average path radiance in the interval (830 $cm^{-1}$; 1250 $cm^{-1}$) in matrix form as follows:

$$Lpath_{avg} = \frac{[Lpath(\nu_1) \quad Lpath(\nu_2) \quad \cdots \quad Lpath(\nu_{84}) \quad Lpath(\nu_{85}).]}{(1250-830)} \cdot \begin{bmatrix} \Delta\nu_1 \\ \Delta\nu_2 \\ \vdots \\ \Delta\nu_{84} \\ \Delta\nu_{85} \end{bmatrix} \tag{5.5}$$

Another term that it is commonly used is the Integrated Radiance, defined as:

$$Lpath_{Tot} = \left[Lpath(\nu_1) \quad Lpath(\nu_2) \quad \cdots \quad Lpath(\nu_{84}) \quad Lpath(\nu_{85}).\right] \begin{bmatrix} \Delta\nu_1 \\ \Delta\nu_2 \\ \vdots \\ \Delta\nu_{84} \\ \Delta\nu_{85} \end{bmatrix} \quad (5.6)$$

Having found the total radiance, Equation 3.3 can be used to find the apparent temperature. The solution of this equation should be done interactively as was done in subroutine *RtoT( )* of SeaRad.

Subroutine *RtoT( )* in SeaRad computes the apparent black body temperature corresponding to a selected radiance by an iterative process. Starting with a "guessed" temperature, the corresponding output radiance is calculated, and the input corrected until the output matches the required radiance within a selected error range.

## B. SKY RADIANCE ADJUSTMENT

The sky path radiance dependency on the zenith angle alone will impose the condition that the sky temperature will also be dependent only on the zenith angle. This means that at the horizon, as an example, a unique value of an apparent black body temperature can be found and used to compare with the temperature read directly from the image plane and also used to adjust the sky radiance.

Using the default meteorological range, with sea temperature of 17.5 °C, air mass character 3, no clouds or rain condition and using the observer zenith angle to the horizon, that is: 90.15°, then the execution of SeaRad will result in the plot of Figure 5. 3.

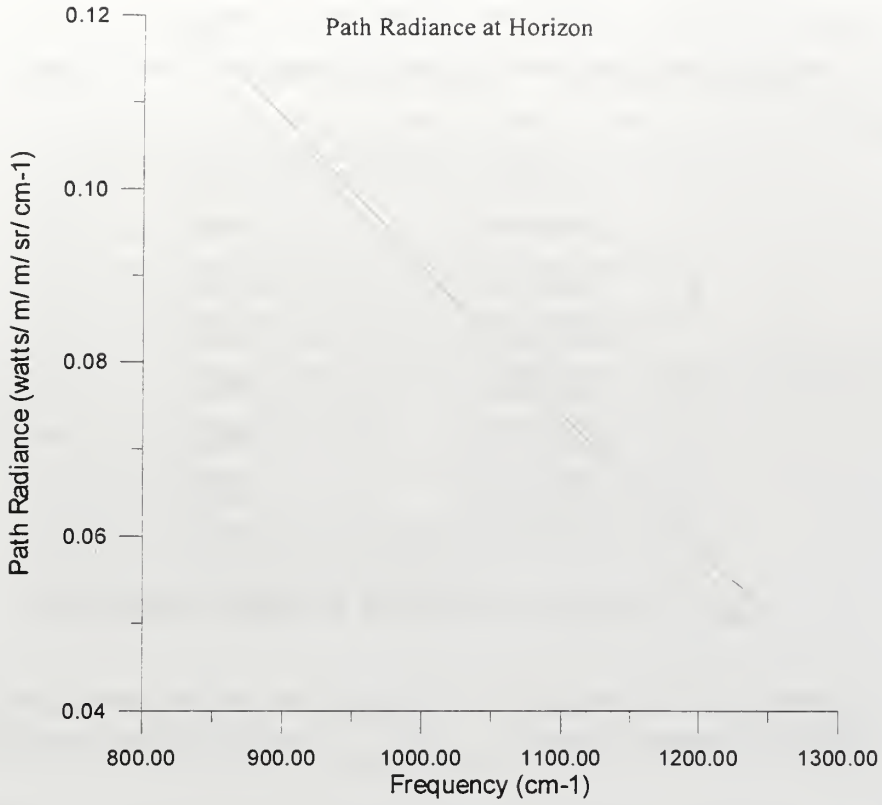


Figure 5. 3 Smaller Sky Path Radiance Condition.

Note from Table 4. 4, that the ICSTL=3 case gives close to the lowest radiance values. Using that radiance as input for Equation 3.3, and solving it for the apparent black body temperature, a value of 21.4 °C is found.

Thus, the SeaRad result is higher than the expected values of 18.3± 1.7 °C (Figure 4. 10) by a nominal value of 3.1 °C.

Since just changing the SeaRad parameters for this specific case cannot decrease the path radiance further, the solution is to offset the path radiance by a constant radiance value.

Taking the path radiance vector "*Lpath*" from Figure 5. 3, the required offset can be estimated by the following process:

- Guess an offset.
- Change vector *Lpath* to *Lpath* = *Lpath* – *offset*n*; where n is an integer.
- Apply Equation 3.3 to find the average black body temperature over the frequency band.

Using SeaRad, the results of Table 5. 1 can be obtained. By interpolation from this table the offset needed to correspond to the required temperature of 18.3 °C is found to be 5.76 $10^{-4}$ watts/cm$^2$.

| Offset (watts/cm$^2$) | Average Temperature (°C) |
|---|---|
| 2.2601e-004 | 20.21 |
| 3.3901e-004 | 19.63 |
| 4.5201e-004 | 18.99 |
| 5.6502e-004 | 18.36 |
| 6.7802e-004 | 17.78 |
| 7.9102e-004 | 17.15 |

Table 5. 1 Finding the Correction for SeaRad Path Radiance.

This offset can also be written in $\frac{watts}{m^2.sr.cm^{-1}}$ using the following equation:

$$path\_offset = 5.76\ \ 10^{-4}\frac{watts}{cm^2} = 5.76\ \ 10^{-4}\frac{1}{5 \bullet .\pi \bullet 10^{-4}}\frac{watts}{m^2 \bullet sr \bullet cm^{-1}} \qquad (5.7)$$

Where: It was assumed $\Delta v = 5cm^{-1}$. Thus, the offset of 5.76e-4 watts/cm$^2$ should be added to all sky path radiance in all the SeaRad calculations that will follow this section.

## C. SEA RADIANCE ADJUSTMENT

Like the sky path radiance, the sea radiance can also be adjusted since we usually know the sea temperature. The idea here is to calculate the reflected and emitted radiances that leave from a given sea position at a given apparent black body temperature read from the meteorological data. Adding the radiances introduced by the atmospheric propagation, the apparent temperature at the observer position can be found and compared with the value read directly from the image plane. If there is no difference in the compared temperatures, then no correction is needed; otherwise a similar procedure to that used in the previous section should be applied.

From Figure 4. 4, the target position relative to the observer has a zenith angle of 90.83°. Using this angle and all other inputs from the previous section, we can build the following 85 component radiance vectors by running SeaRad, all in $\frac{watts}{m^2 \bullet sr \bullet cm^{-1}}$:

- Footprint to observer path radiance: *Lp = SUMT.*
- Sun reflected on the sea at zero range (leaving footprint): *Lsuno = Nvo.*
- Sun reflected on the sea at full range (reaching observer): *Lsun = Nvo.Tau(I).*
- Sea emission at zero range: *Lseao = e.Nbb.*
- Sea emission at full range: *Lsea = e.Nbb.Tau(I).*
- Sky reflection at zero range: *Lrskyo = Nvsky.*
- Sky reflection at full range: *Lrsky = Nvsky.Tau(I).*

In the above radiances, the left side of the expression is the variable definition, and the right side is its SeaRad interpretation, where:

- e = sea emissivity.
- Tau(I) = atmospheric transmissivity.
- Nbb = Planck's black body radiance.

Comparing those variables with Equation 3.5 and Equation 3.10, we identify:

$$Lrskyo = \rho_o \bullet L_{sky} \tag{5. 8}$$

$$Lsuno = \tau_s \bullet L_s \tag{5. 9}$$

$$Lseao = \frac{C_1}{\pi \bullet \lambda^5} \bullet \frac{\varepsilon_{sea}}{e^{\frac{C_2}{\lambda \bullet T_{sea}}} - 1} \tag{5. 10}$$

Writing for zero range sea radiance:

$$Lo = Lseao + Lrskyo + Lsuno \tag{5. 11}$$

Considering the sky path radiance correction of Equation 5.7, we will have after its reflection on the sea, using the polynomial form of Equation 4.7 for $\rho_o$ :

$$sky\_correc = \rho_o\left(\pi - 90.83^o\right) \bullet 5.76 \bullet \frac{1}{5 \bullet \pi} \tag{5. 12}$$

$$Lo = Lseao + \left(Lrskyo - sky\_correc\right) + Lsuno \tag{5. 13}$$

And for full range:

$$Lo@camera = Lo \bullet \tau + Lp = Lsea + Lrsky - sky\_correc + Lsun + Lp \tag{5. 14}$$

For this experiment date the sky was overcast and in consequence the *Lsun* component can be neglected, simplifying the previous equations.

As was done in the previous section, by application of Equation 3.3, using Equation 5.14 as input, the apparent black body temperature at the observer position can be found. The sea

footprint position was kept constant at a zenith angle of 90.83° relative to the observer. The results are shown in Table 5. 2.

| **Sea Temperature (°C) (Tbound)** | **Calculated Apparent Temperature Seen by AGA (°C)** |
|---|---|
| 14.5 (thermistor) | 12.6 |
| 17.6 (Metoc) | 13.4 |
| 16.05 (average) | 13.0 |

Table 5. 2 Temperature Attenuation for the Ship Position.

Comparing the Table 5. 2 results with Figure 4. 5, and considering that the average Tbound temperature provides the correct apparent temperature for the sea at the ship position, no extra radiance compensation is necessary.

To see the influence of the path radiance as the observer zenith angle approaches the horizon, Figure 5. 4, for an observer zenith angle of 90.2°, and Figure 5. 5, for an observer zenith angle of 90.85°, were plotted. In both figures the same sea temperature *Tbound=289.6* ℃ was used. It can be inferred that the increase of path radiance, as the observer zenith angle approaches the horizon, is the main reason for the increase in the apparent temperature at the observer position.

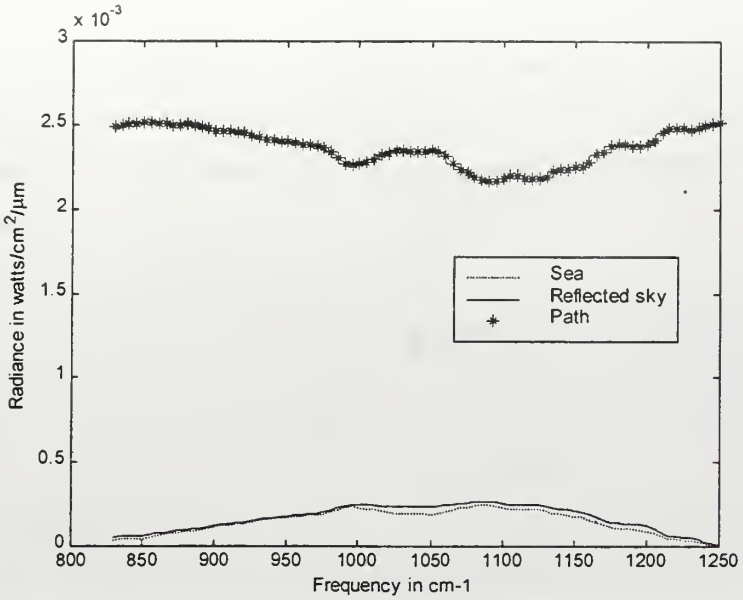


Figure 5. 4 Radiance Near the Horizon. Observer Zenith Angle of 90.2°.

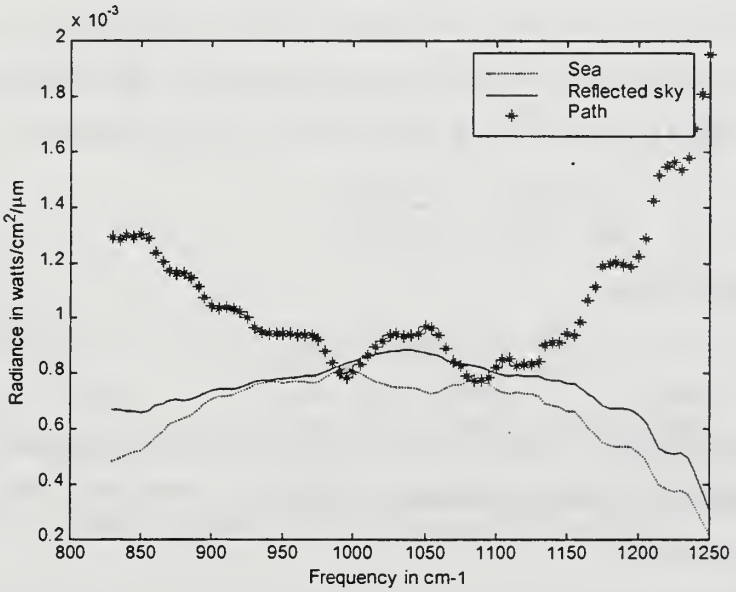


Figure 5. 5 Radiance for Near the Target Position. Observer Zenith Angle of 90.85°.

## D. THE TEMPERATURE DISTRIBUTION IN THE IMAGE PLANE

Assuming a plane earth, Figure 5. 6 can be used to find the relation between each observer zenith angle $\alpha$ and the horizontal projection distance $x$, or between $\alpha$ and the row numbers $p$ in the image plane. Here the subscript H refers to the horizon and the subscript N to the nearest point that the AGA sensor can see (bottom of the image).

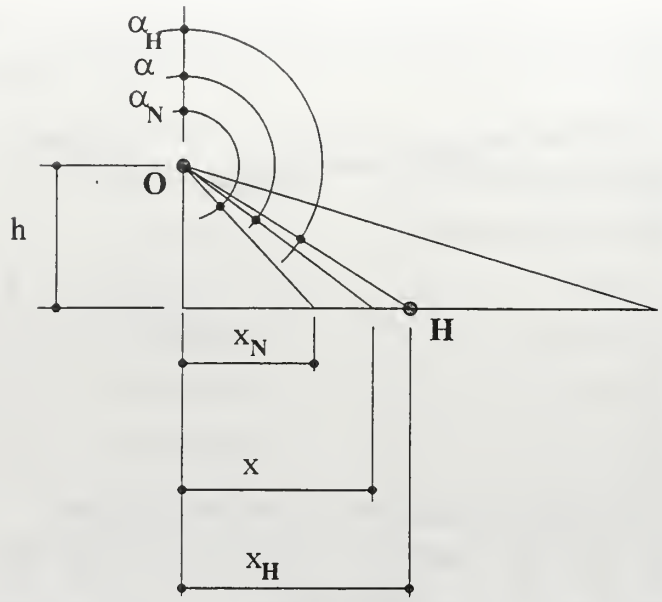


Figure 5. 6 Correspondence Between Zenith Angle and Horizontal Distance. Geometry in Vertical Plane.

The data $(\alpha_N, \alpha, \alpha_H)$ can be associated linearly with the counterparts $(p_N, p, p_H)$, in the image plane. The p value is an image frame characteristic. The PTRWIN files have 256 lines and 125 or 250 pixels per line. Then, p varies from 1 to 256 (1 at the top and 256 at the bottom).

$$\frac{\alpha - \alpha_N}{\alpha_H - \alpha_N} = \frac{p - p_N}{p_H - p_N} \tag{5. 15}$$

And finally write:

$$p = \frac{(\alpha - \alpha_N) \bullet (p_H - p_N)}{\alpha_H - \alpha_N} + p_N \tag{5. 16}$$

Comparing Figure 5. 6 and Figure 4. 4 and analyzing the image plane using the PTRWIN software for example, the following data can be found:

- $p_N = 256.$
- $p_H = 152.$
- $\alpha_N = 93.024^o$
- $\alpha_H = 90.168^o$
- $90.168^o \leq \alpha \leq 93.024^o$

For each p value there is a corresponding pixel value in digital level. Using Equation 2.3 each digital level can be transformed into Isothermal Units, and finally, by using Equation 2.1

the temperature associated with each p value, that is $T(p)$, can be found. The plot of $T(p)$ as a function of the observer zenith angle $\alpha$ is presented in Figure 5. 7, for column 64. Note that the calibration correction is not applied yet, and that column 64 corresponds to the direction that contains the hottest ship point. There is, the ship hottest point is contained on the vertical plane, depicted on Figure 5. 7.

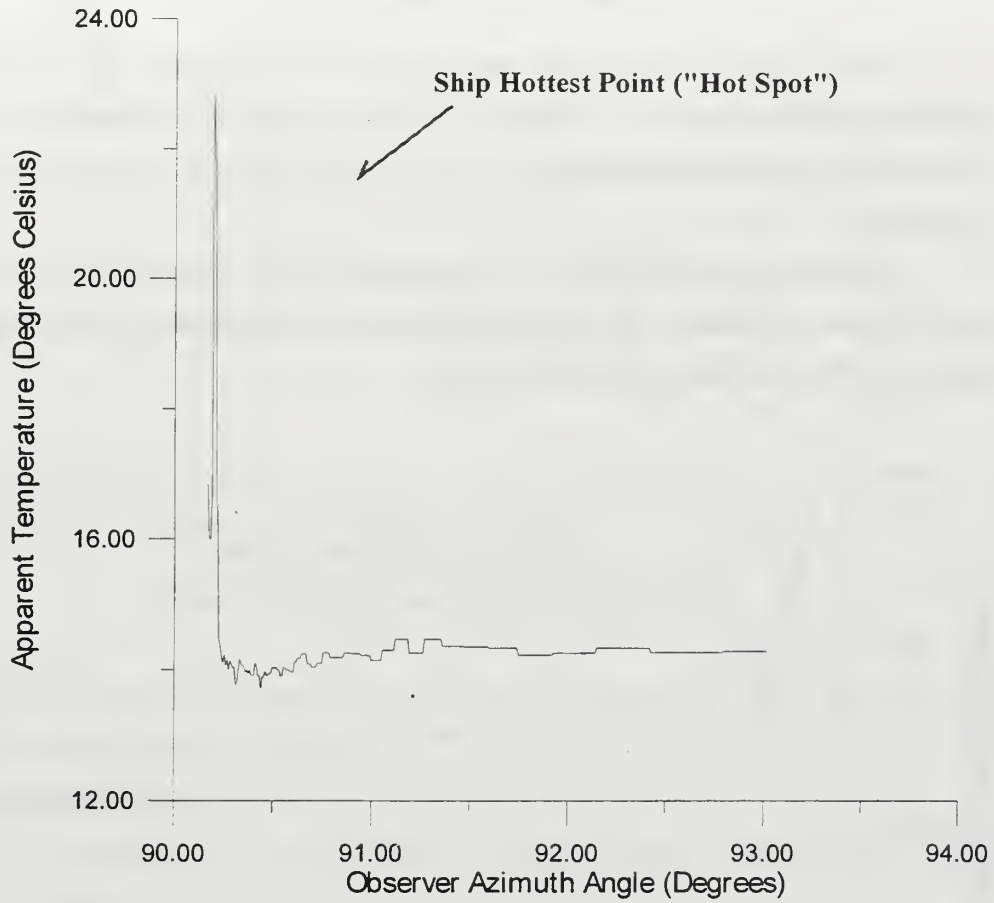


Figure 5. 7 Apparent Temperature Distribution Versus Observer Zenith Angle for the Vertical Plane (Column 64) That Contains the "Hot Spot".

## E. DETERMINATION OF THE "REAL" SEA TEMPERATURE

When we look at the sea near the horizon, the sky reflection dominates the sea emission component and the sea temperature will look lower than it really is. That temperature is referred to as the apparent black body temperature and it corresponds to the sea "Tbound" SeaRad variable. Actually it is an apparent temperature because it includes all radiation leaving the sea and not just the sea emission, this latter being associated with the real temperature of the sea.

To find the apparent black body sea temperature, SeaRad can be used with a little modification on the subroutine *RtoT( )* to consider the sky correction, Equation 5.12. A

dimensional change is necessary, and it can be done by just subtracting the sky correction from the total radiance in $\frac{watts}{cm^2 \bullet sr}$.

Then, for *RtoT( )* the sky correction is:

$$sky\_correc = (1 - esea) \bullet 5.76 \bullet \frac{1}{\pi} \qquad (5.17)$$

Where: *esea* is the average sea emissivity also calculated from SeaRad, applying Equation 5.4 to the emissivity variable "*e*". Now, keeping the sea temperature constant and varying the observer zenith angle, Figure 5. 8 can be constructed by running SeaRad with the sky correction.

By plotting together Figure 5. 7, corrected for AGA calibration, and Figure 5. 8, and using the same coordinates, the apparent sea black body temperature can be read directly from Figure 5. 9, from the intersections of the curves.

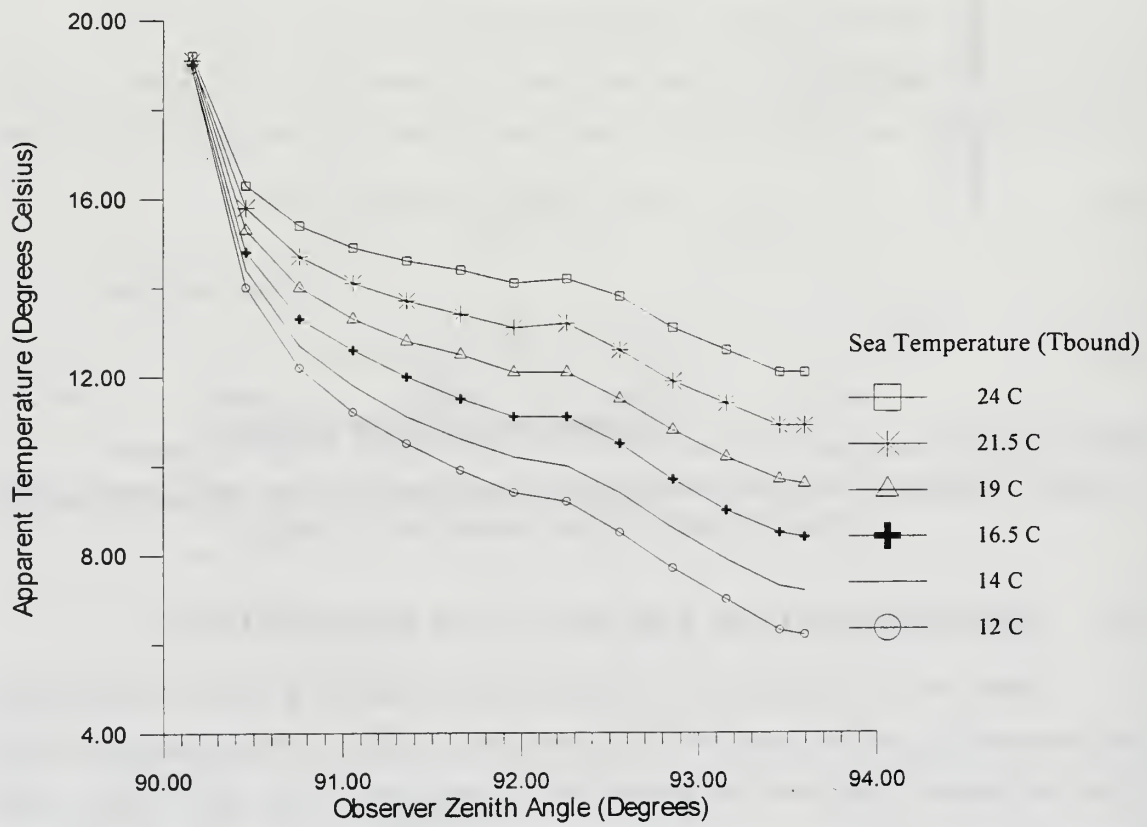


Figure 5. 8 Sea Apparent Temperature at Observer Plane Versus Observer Zenith Angle with Sea Apparent Temperature at Sea Plane as Parameter.

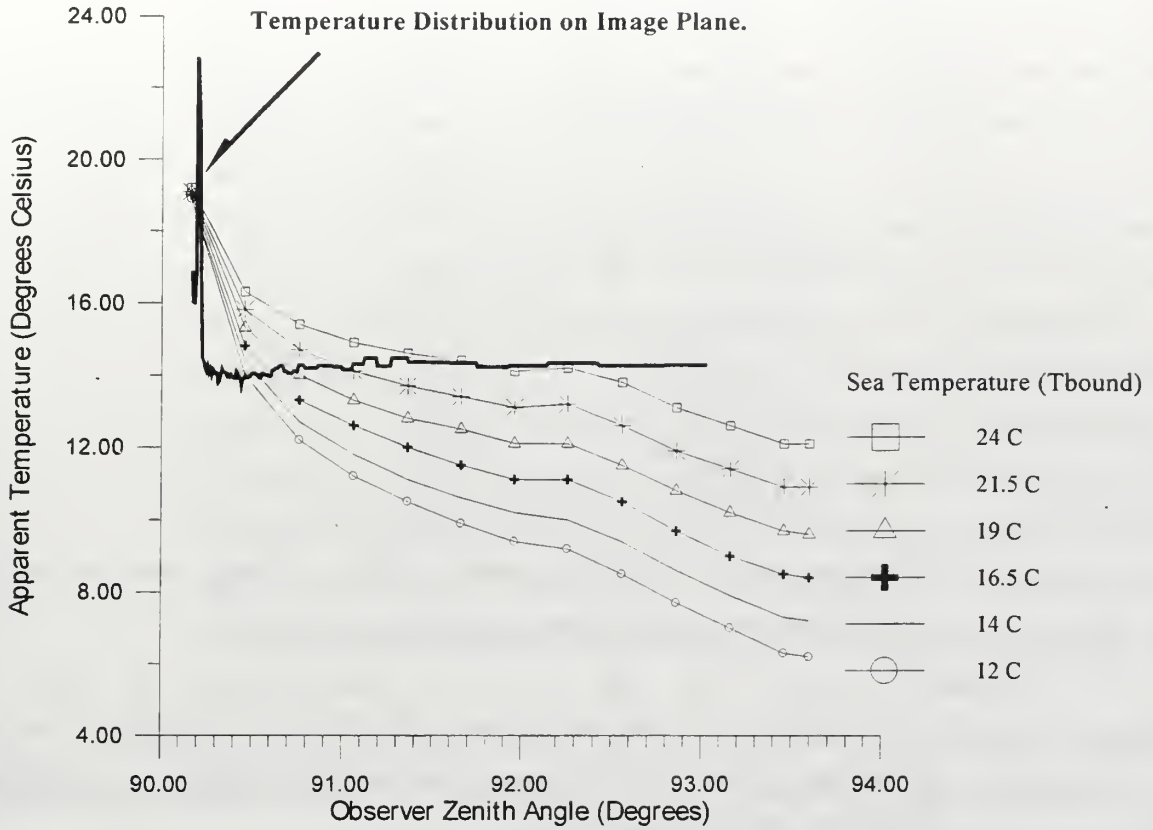


Figure 5. 9 Finding the "Real" Sea Temperature.

The above method will become tedious when processing an image with 256 by 125 pixels, and an automatization is required.

The idea is very simple:

- Use Equation 2.3 to transform the original image in digital level to isotherm units.
- Use Equation 2.1 to transform the isothermal unit image into a temperature image, called a *T_image*. This image file will have dimension 256 rows by 125 columns.
- Correct *T_image* in order to take into account the calibration error by adding to all its elements the nominal error 2.3 °C.
- Define the vector $\overline{\alpha}$. Its elements should be in the range $90.16^o \le \alpha \le 93.02^o$. Also, find the corresponding $\overline{p}$ vector, using Equation 5.16.

$$\bar{\alpha} = \begin{bmatrix} 90.16^0 \\ 90.46^0 \\ 90.76^0 \\ 91.06^0 \\ 91.36^0 \\ 91.66^0 \\ 91.96^0 \\ 91.26^0 \\ 92.56^0 \\ 92.86^0 \\ 93.02^0 \end{bmatrix} \rightarrow \bar{p} = \begin{bmatrix} 152 \\ 163 \\ 174 \\ 184 \\ 195 \\ 206 \\ 217 \\ 228 \\ 239 \\ 250 \\ 256 \end{bmatrix}$$

- Define the vector of sea *Tbound* values. Here 11 values were selected, but *Tbound*, *p* or $\alpha$ can have any size and any values of interest.

$$Tbound = \begin{bmatrix} -263.15 & -70 & -20 & 0 & 12 & 14 & 16.5 & 19 & 21.5 & 24 & 40 \end{bmatrix}$$

- Now, as before, by running SeaRad with the sky correction for the sea temperature Tbound and the observer zenith angle α, Figure 5. 8 can be plotted again or the following matrix built:

$$Tapp = \begin{bmatrix} 17.8 & 17.9 & 18.4 & 18.7 & 18.9 & 18.95 & 19 & 19.1 & 19.15 & 19.2 & 19.6 \\ 3.3 & 4.7 & 9.1 & 12 & 14 & 14.4 & 14.8 & 15.3 & 15.8 & 16.3 & 19.7 \\ -3.3 & -1.3 & 5.2 & 9.3 & 12.2 & 12.7 & 13.3 & 14 & 14.7 & 15.4 & 20.1 \\ -7.3 & -4.9 & 2.9 & 7.8 & 11.2 & 11.8 & 12.6 & 13.3 & 14.1 & 14.9 & 20.4 \\ -10.5 & -7.7 & 1.2 & 6.7 & 10.5 & 11.1 & 12 & 12.8 & 13.7 & 14.6 & 20.6 \\ -13 & -9.9 & -0.1 & 5.8 & 9.9 & 10.6 & 11.5 & 12.5 & 13.4 & 14.4 & 20.9 \\ -15.4 & -12 & -1.4 & 5 & 9.4 & 10.2 & 11.1 & 12.1 & 13.1 & 14.1 & 21 \\ -17 & -13.3 & -2.1 & 4.7 & 9.2 & 10 & 11.1 & 12.1 & 13.2 & 14.2 & 21.4 \\ -19.2 & -15.3 & -3.4 & 3.7 & 8.5 & 9.4 & 10.5 & 11.5 & 12.6 & 13.8 & 21.2 \\ -21.5 & -17.4 & -4.8 & 2.7 & 7.7 & 8.6 & 9.7 & 10.8 & 11.9 & 13.1 & 20.8 \\ -22.7 & -18.0 & -5.5 & 2.1 & 7.3 & 8.2 & 9.3 & 10.5 & 11.6 & 12.8 & 20.7 \end{bmatrix}$$

Each column "J" of *Tapp(*,J)* corresponds to *Tbound(J)*, and each row "I" of *Tapp(I,*)* corresponds to *p(I)* or equivalently to $\alpha(I)$.

Where: * means all elements.

- The key point here is that at each *p(I)* coordinate, *Tapp(I,*)* can be applied over all pixels in all columns of this row (see Chapter IV.B.3). Then the problem resumes in finding the vector *Tapp_row* by interpolation, corresponding to each

integer row number *p'* of the image plane from 152 to 265. As an example, for row *p'*=152: *Tapp_row* = *Tapp(1,*)*, and for row *p'*=153: *Tapp_row* should be interpolated between *Tapp(1,*)* and *Tapp(2,*)*, knowing that in this interval *p(I)* varies between 222 and 152.

- The *Tapp_row* value obtained for the specific row *p'* can be applied for each *T_image(p',*)* element to find the corresponding Tbound element. This is an easy task because each column of *Tapp* is associated with a *Tbound* element.
  As an example, assume *p'*=152. Then *Tapp_row* = *Tapp(1,*)*, and interpolation over all 125 elements of row 152 of *T_image* matrix is needed, that is, T_*image(p',*)*. To interpolate a hypothetical T_*image(p',20)=18.8* ℃, for instance, it can be seen that 18.8 is between *Tapp(1,4)=18.7* and *Tapp(1,5)=18.9* and the corresponding Tbound varies from *Tbound(4)=0* to *Tbound(5)=12*. Thus, the corresponding sea Tbound value for the apparent temperature of 18.8 °C is 6°C.

In the above procedure, from [Ref. 2], the sky was considered as having an apparent black body temperature of –40 °C. This is necessary to put a lower limit in the calculations.

Also, the range compensation for the ship pixels should be discarded because their distance to the observer is almost constant, and the ship emits a different spectrum of radiation from the sea. The ship will be range-compensated in the next section.

The ship temperature is very prominent in Figure 4. 5 with respect to its surroundings. Thus, the ship pixel coordinates can be found easily and a mask can be built as in Figure 5. 10

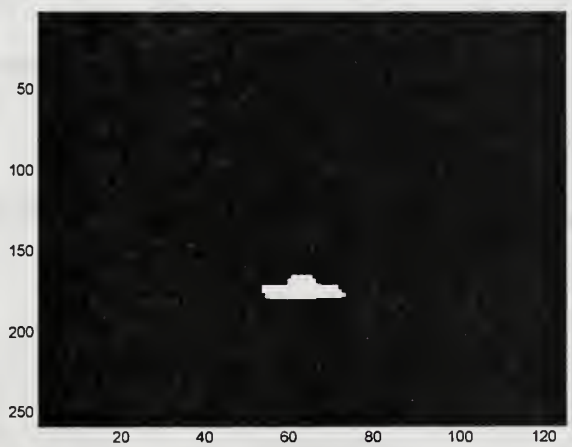


Figure 5. 10 Ship Mask.

The final range compensation, missing only the ship correction, is shown in Figure 5. 11.

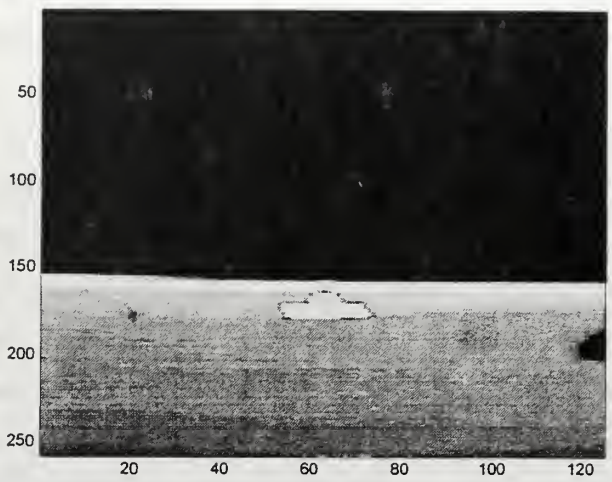


Figure 5. 11 Range Compensation for the Sea.

Another ship can be seen on the right side of Figure 5. 11. Its range compensation is also wrong for the same reason as for the main target discussed previously. But, it does not have any kind of relation with this thesis, and in consequence it will not be corrected.

## F. RANGE COMPENSATION FOR THE SHIP

From Figure 3. 4 and Equation 3.10, Equation 5.18 can be written:

$$L_t = t\,arg\,et\_emission + \rho_t \bullet \left(Lo + Lsky + \tau_s \bullet Ls\right) \tag{5. 18}$$

*Ls* is almost zero because of the overcast condition, and before any radiance correction *Lo* is given by Equation 5.11 and *Lsky* by Equation 5.8. Hence, calling *Lte* the *target_emission*:

$$L_{to} = Lteo + \rho_t \bullet \left( \left(Lseao + Lrskyo + Lsuno\right) + \frac{Lrskyo}{1-e} \right) \tag{5. 19}$$

Finally, considering the sky correction from Equation 5.12:

$$Lt\_reflo = \rho_t \bullet \left( \left(Lseao + Lrskyo - sky\_correc + Lsuno\right) + \frac{Lrskyo - sky\_correc}{1-e} \right) \tag{5. 20}$$

$$L_{to} = Lteo + Lt\_reflo \tag{5. 21}$$

$$L_t @ camera = L_{to} \bullet \tau + Lp = Lte + Lt\_refl + Lp \tag{5. 22}$$

$$Lt\_refl = \rho_t \bullet \left( \left(Lsea + Lrsky - sky\_correc + Lsun\right) + \frac{Lrsky - sky\_correc}{1-e} \right) \tag{5. 23}$$

All the components of *Lt_refl*, *Lp and* $\tau$ can be obtained using SeaRad, as was done before. For the target emission calculation the ship average temperature can be found using the ship mask.

But, a better solution is to find the radiance *Lt@camera* corresponding to different temperatures on the target and apply Equation 3.3 to find the apparent target temperature at the observer position. Comparing with the previous sea procedure, this is equivalent to finding just a one row *Tapp* vector for the target.

To find *Lt_refl*, *Lp and* $\tau$, SeaRad must be run just one time because all the ship points are assumed to have the same distance to the observer, and *Lt_refl*, *Lp and* $\tau$, are functions of the sea temperature instead of the target temperature. The main input parameters for SeaRad are:

- Tbound = 16.04 °C.
- Observer zenith angle = 90.83°.

Now, applying a target version of Equation 5.10 to find the target emission, for $\varepsilon_{ship} = 0.95$, from Chapter III.C.1.

$$Lteo = \frac{C_1}{\pi \bullet \lambda^5} \frac{0.95}{e^{\frac{C_2}{\lambda \bullet T_{ship}}} - 1} \tag{5.24}$$

For a target temperature of 12 °C, the radiance distribution in frequency for the ship is plotted in Figure 5. 12.

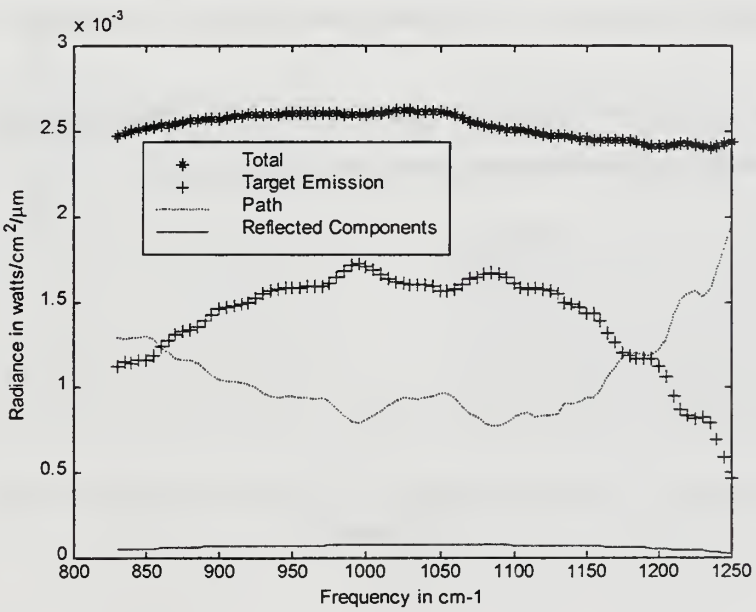


Figure 5. 12 Observed Radiance From the Ship Position. The Reflected Components are Small Compared to the Emission, but the Contribution of Path Radiance is Significant.

Applying Equation 3.3 to Equation 5.23, for different ship temperatures, the corresponding in-band average apparent temperature at the observer position can be found. The results are in Table 5. 3.

| **Target Temperature Tbound (°C)** | **Target Apparent Temperature (°C)** |
|---|---|
| 10.0 | 15.35 |
| 12.0 | 16.47 |
| 14.0 | 17.65 |
| 16.0 | 18.83 |
| 18.0 | 20.00 |
| 20.0 | 21.18 |
| 22.0 | 22.42 |
| 24.0 | 23.60 |
| 26.0 | 24.84 |
| 28.0 | 26.08 |
| 30.0 | 27.32 |

Table 5. 3 Mapping of Apparent Ship Temperature to Ship *Tbound* Temperature.

Applying the ship mask,

Figure 5. 10, to the AGA image, only the ship pixels can be extracted. Applying Table 5. 3 to those pixels, the mapping of the apparent temperature to the target *Tbound* temperature can be done.

Figure 5. 13 shows part of the data of column 64 of the compensated image, after the mapping of the ship apparent temperature to *Tbound* temperature.

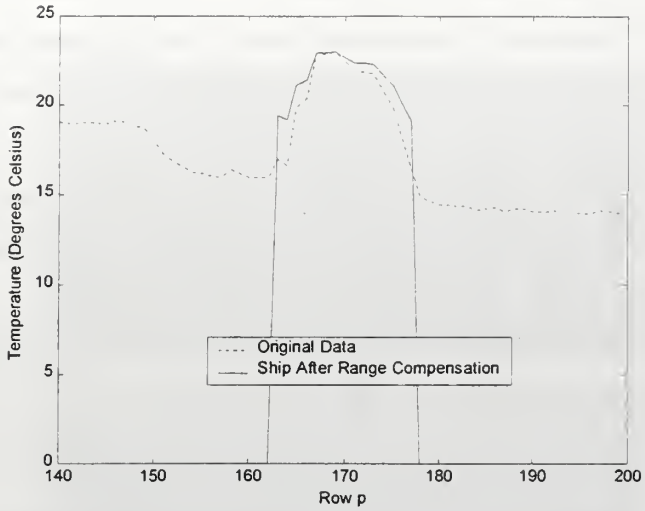


Figure 5. 13 Comparison of the Range-compensated Temperature and Original Apparent Temperature Data for the Ship before any Sea-Ship Interface Correction. Image Plane Sectioned at Column 64.

The superposition of the range compensation for the ship and for the sea , for the same column 64 of the compensated image is represented on Figure 5. 14.

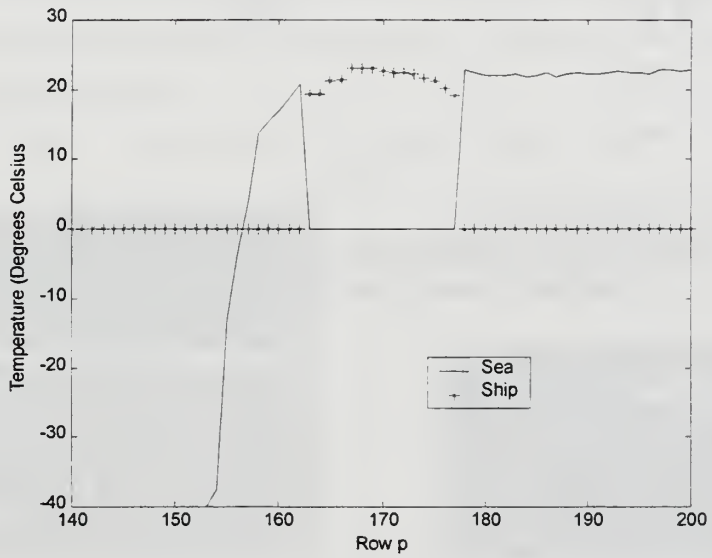


Figure 5. 14 The Discontinuity of Temperature at Sea-Ship Interface. Image Plane Sectioned at Column 64.

Figure 5. 14 shows that an adjustment is needed to correct the discontinuity in the sea-ship interface. This continuity should occur only on the right interface side, that is, the region nearest to the observer, where the observer sees the hull of the ship encounter the sea.

The procedure to adjust the ship temperature is:

- Define a column that contains ship data. As an example, take column 64.
- In that column, find the rightmost row number, *correction_row*, where the ship temperature is bigger than zero.
- The temperature correction is: [Sea temperature at row (*correction_row+1)*] – [ship temperature at row *correction_row*].

The result is shown in Figure 5. 15 and Figure 5. 16.

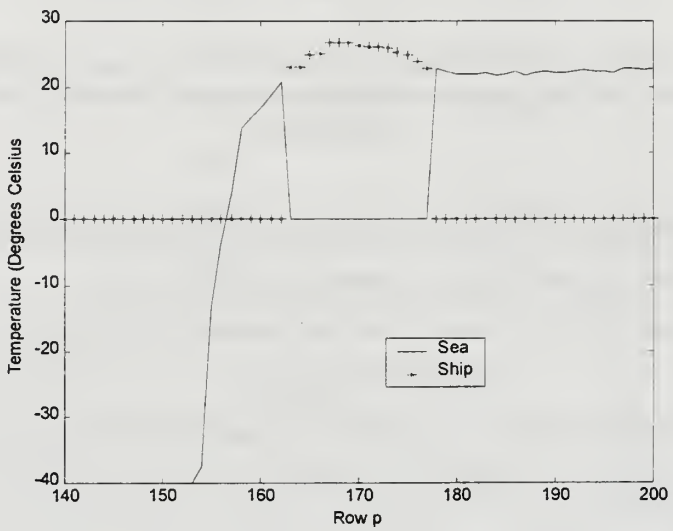


Figure 5. 15 Ship Temperature distribution after Discontinuity Correction at the Sea-Ship Interface. Image Plane Sectioned at Column 64.

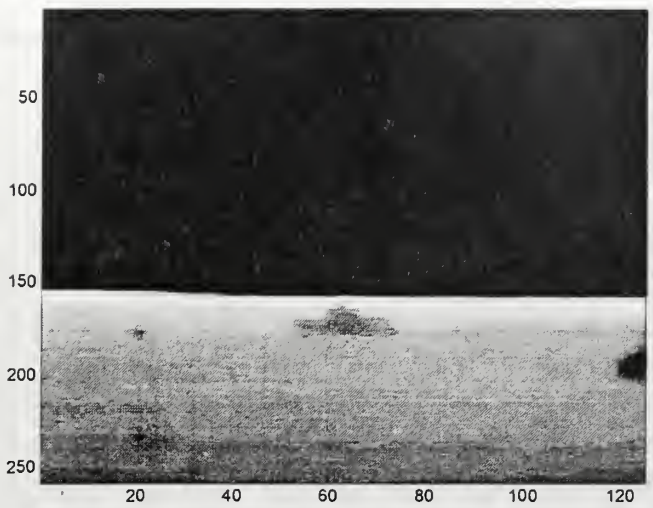


Figure 5. 16 The Final Image After the Application of the Range Compensation Method. This Image represents the Apparent Black Body Temperature at Source Origin Position.

## G. ANALYZING THE RESULTS

A visual comparison of the compensated and the original image, Figure 5. 17, shows that a better way to analyze the images must be found. Here, it was chosen to section the image in the vertical and horizontal directions.

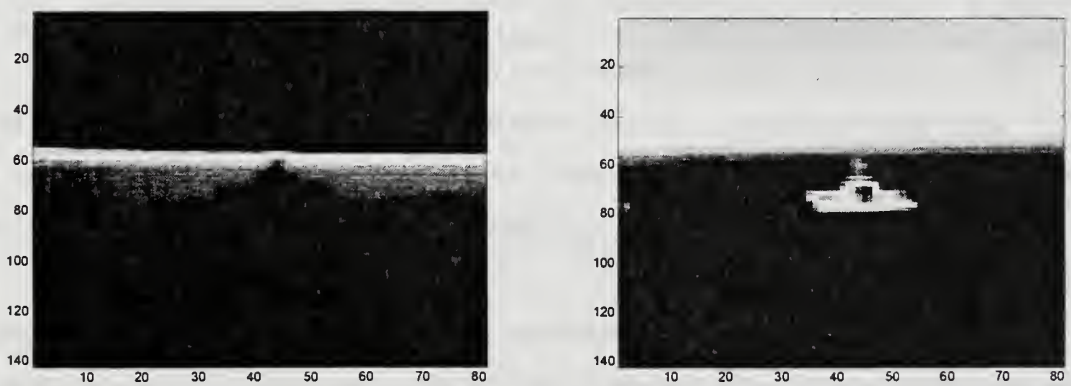


Figure 5. 17 Left is the Compensated Image, Right is the Original Image.

In the vertical direction, Figure 5. 18, the ship temperature has become more flattened. This is due to the fact that for small target *Tbound* the path radiance has a great influence on

temperature attenuation and it is responsible for the small values of the temperature difference $\Delta T$ between *Tbound* and its corresponding apparent temperature. Since the atmospheric parameters are kept constant for the ship compensation, and the only changing factor is the ship emissivity, then as *Tbound* increases its influence becomes dominant over the path radiance. In consequence there will be a temperature at which there will be a transition from one situation to another and where $\Delta T = 0$. From Table 5. 3, that temperature is near 23 °C. Since most of ship data are around 23 °C this explains the flatness of the ship compensation results.

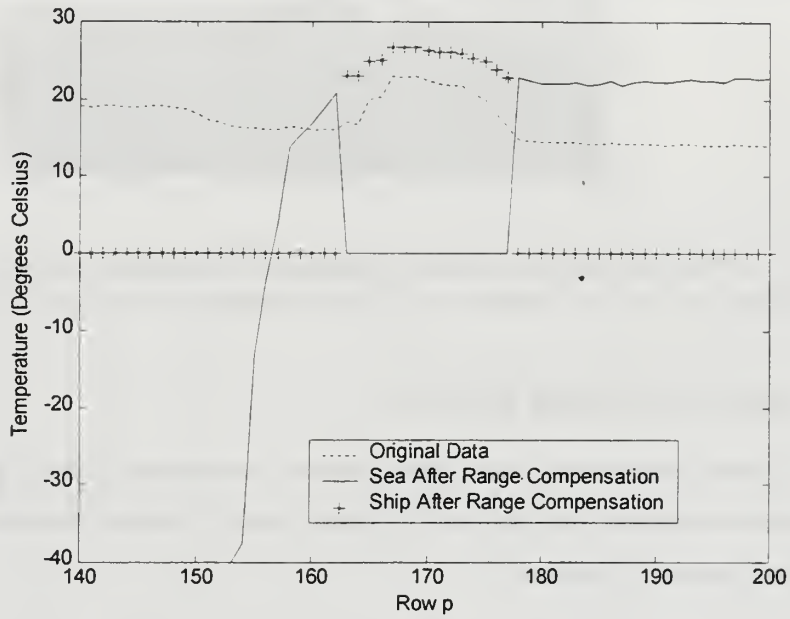


Figure 5. 18 Comparing The Results of The Image After the Range Compensation. The Ship Temperature Distribution Has Become Flattened and the Gradient of the Sea Temperature Near Horizon Very Accentuated.

Also note from Figure 5. 18, how accentuated is the path radiance on the sea $\Delta T$ near the horizon, where the sea temperature approaches the sky temperature.

Far from the horizon and near to the observer the path radiance is smaller, so that less $\Delta T$ correction is necessary.

In image row coordinates, the ship is near the horizon and because $\Delta T$ there is higher, it is expected that the contrast in the horizontal direction will be improved. This improvement can be seen by sectioning Figure 5. 16 horizontally at different rows containing the ship pixels, as is done in Figure 5. 19 to Figure 5. 22.

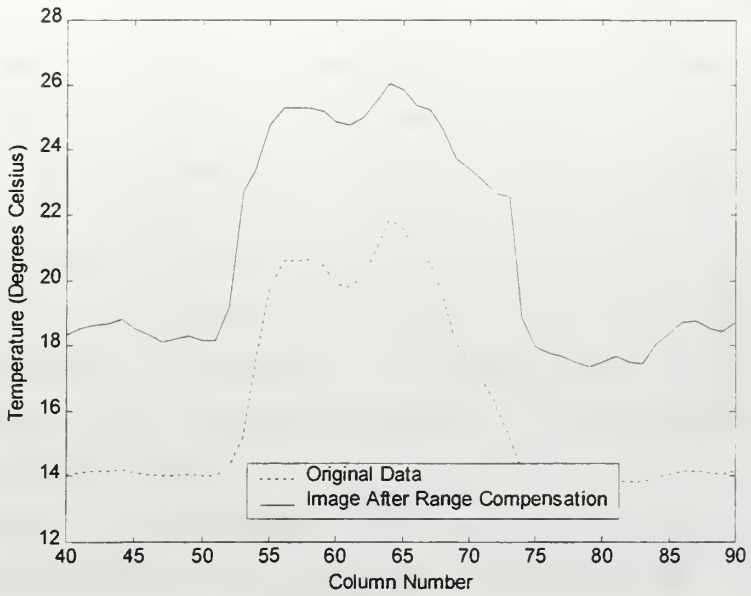


Figure 5. 19 Ship-Sea Contrast for Row 172 (Position Far From the Horizon Row: 152). No Visible Improvement in the Contrast.

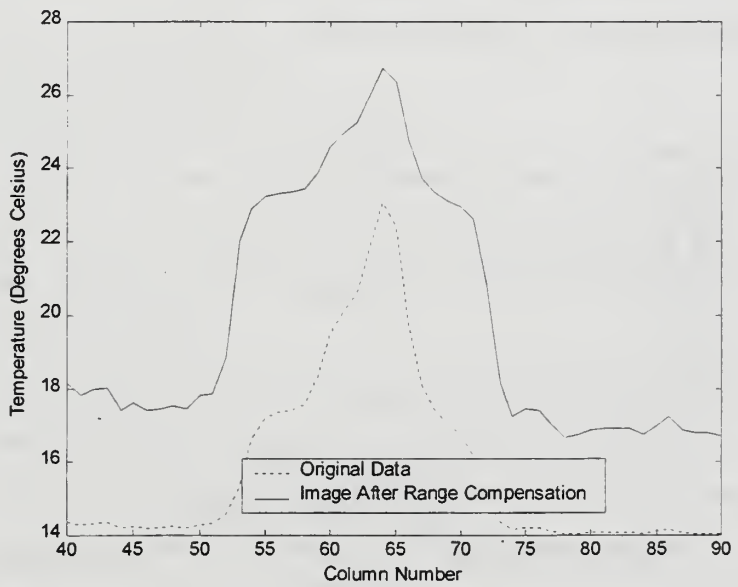


Figure 5. 20 Ship-Sea Contrast for Row 169. Still No Visible Improvement in the Contrast.

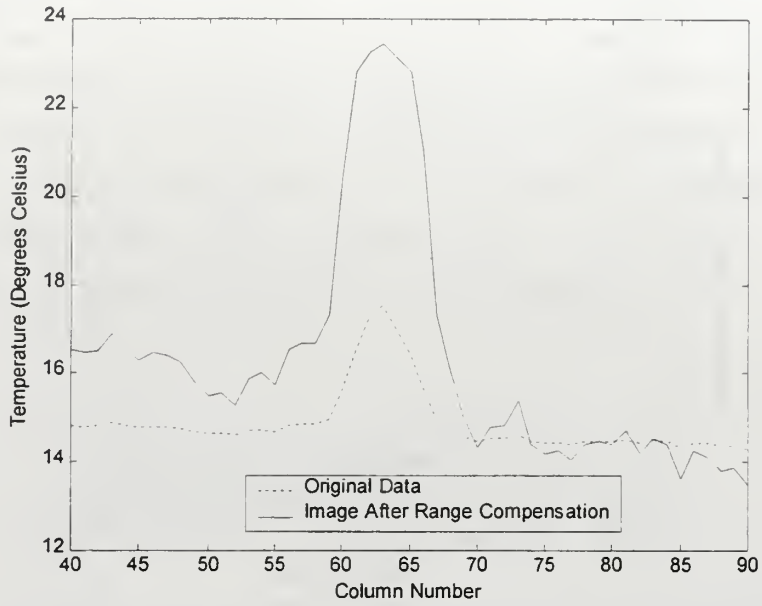


Figure 5. 21 Ship-Sea Contrast for Row 163. The Contrast is Improved as the Ship Pixels are Contrasted with the Sea Pixels Near the Horizon.

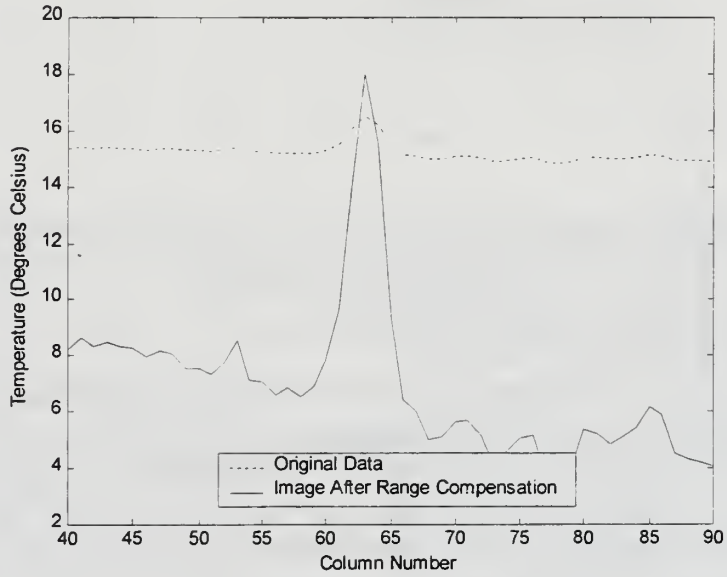


Figure 5. 22 Ship-Sea Contrast for Row 159, a Position Very Near to the Horizon (Row 152). The Improvement in the Contrast is Intensified.

# VI. CONCLUSIONS AND RECOMMENDATIONS

The equipment calibration is the first difficulty in working with thermal vision data. The correct calibration will allow the correct transformation from the equipment-dependent parameters to the real world temperature scale. But in order to find that calibration curve a calibration data point associated with the experiment data should exist. That is, black body measurements interpolated between the image measurements should exist. Having those data to check, it should be easy to adjust the controller output to reset it to the conditions of the time of the experiment and find in the laboratory the correct calibration curve. Then, using this correct calibration and using the same black body measurements the error and the dispersion associated with the experiment can be found.

In this thesis, an error of -2.3 ± 1.7 °C was found for unpolarized images. This magnitude represents about a 10 % error in the mean. This error was used to offset all the image pixels after the application of the correct calibration curve.

To develop a range compensation method is not an easy task due to the complex mechanisms of the radiation interaction, the randomness of sea wavelets, and because it requires knowledge of the theory that involves atmospheric constituents, optical and solar path, sun position and the model of scattering. Then, the second step in the solution of the problem involves same simplifying assumptions.

The following simplifications were assumed:

- All sources were extended Lambertian sources. This allows introducing a dependency on solid angle by just dividing or multiplying by $\pi$.
- The emissivity of the research ship R/V POINT SUR was considered constant and equal to 0.95.
- The reflections of the sun radiation from the sea and from the target were neglected due to the overcast condition of the experiment.
- To skip the hard mathematics behind the effects of atmosphere on the generation and attenuation of radiation, the SeaRad program was used.
- Due to the small field of view of the equipment and the big distances involved, the geometry of the problem allows considering all the horizontal pixels in the image plane to have the same distance to the observer. Then, it is necessary to

find the atmospheric parameters as a function of distance in just one particular azimuth direction.

After these simplifications the structuring of the range compensation method was begun by considering that all points located on the ship have the same distance to the observer and that the sky has an indefinite distance to the observer so that the concept of range compensation has lost its meaning. But this same property that the sky radiance is independent of distance allows correction of the SeaRad sky radiance by comparing it to the apparent temperature in the image. For the file "NSD1003.ptw", the offset needed to correct the SeaRad sky radiance output is 5.76e-4 watts/cm$^2$.

The file NSD1003.ptw was chosen as the example for calculation of range compensation because it shows the ideal image conditions for this analysis. That is, that the target is the center of the picture, that the target contour is well defined (good contrast), and the horizon line is sharply defined.

Using SeaRad to calculate the apparent sea temperature *Tapp_sea* at the ship position and comparing it with its corresponding value read from the image file, it was found that no extra radiance correction was necessary for the sea radiance.

The sea can then be range-compensated by first building curves of apparent temperature *Tapp_sea* versus observer zenith angle $\alpha$ for different sea apparent black body temperature *Tbound_sea*. Next, by finding the relation between each observer elevation angle $\alpha$ and the row numbers $p$ in the image plane, the pixels in the image plane can be mapped into curves that use the same scale as *Tapp_sea* versus $\alpha$. Finally by plotting together the previous two graphics, the sea *Tbound* can be read directly from that plot for each intersection point (*Tapp_sea* , $\alpha$). This procedure can be automated by transforming the plot into an 11 by 11 matrix, for example, where each row corresponds to $p$ and each column to *Tbound_sea*.

To range-compensate the ship all that it is needed is to know the ship apparent black body temperature *Tbound_ship* as a function of the apparent temperature *Tapp_ship* at the image plane. This can be done because all the ship points were assumed to have the same distance to the observer, so that $p$ is constant. But a discontinuity correction is needed to adjust the ship temperature to the sea temperature at the sea-ship interface and complete the overall range compensation.

An analysis of the range-compensated image shows that in the vertical direction the ship temperature has become more flattened. This is because the ship temperature is around 23 °C ,

and this temperature is a transitional temperature where *Tbound-ship* become higher than *Tapp_ship*. For temperature less than 23 °C *Tbound-ship* is less than *Tapp_ship*. The basis for that transition temperature is the magnitude of the path radiance.

The path radiance has a great influence on temperature attenuation and it determines the temperature difference between *Tbound* and its corresponding apparent temperature in most$\theta$ cases. This fact is clearly seen near the horizon where the sea temperature approaches the sky temperature, and this will result in a range-compensated image completely different from the original.

The range-compensation method proposed in this thesis has many advantages over the usual integral solving approach to find the original exitance of a source and range-compensate a pixel in the image plane. One is the reduction in the computation time because it is easier to interpolate than solve an integral (or to solve a matrix expression, if we change the continuous integral form into the discrete form). Another advantage of the proposed method is that the same apparent temperature matrix can be used for images taken at another time if the atmospheric conditions did not change dramatically, because in this case the radiance components are unchanged. Also the computer memory needed to solve the problem is much less in this case. Using a matrix form with a 5 $cm^{-1}$ frequency step size to solve the integral, the traditional approach requires the storage of vectors of 85 elements (transmittance, emissivity and radiances) for each row in the sea image plane. Instead, the actual method merely needs to store a matrix of the size of the precision desired (in this thesis an 11 by 11 matrix). But the biggest advantage is the simplicity.

Note that the principal difference between the two methods is the direction of the calculation of the integral that relates the received irradiance with the source exitance. The proposed method uses the source exitance to find the irradiance at the full range in opposition to the traditional method that solves for the radiant source exitance knowing the received irradiance. Then, both methods should give the same results if the number of rows and columns of the apparent temperature matrix are selected in such a way that no interpolation is needed.

In this thesis SeaRad, Matlab, Mathcad, and other data manipulating programs were used. But a unique user-friendly program can be written to find the correct signal and background temperature and use it in predictive codes to estimate the signature at any other range.

Although all this work was conducted for an unpolarized image, the same basic guidelines can also be applied for polarized cases.

This Page Intentionally Left Blank

## LIST OF REFERENCES


1. Cooper, A.W. and Crittenden, E.C., "Electro-Optic Sensors and Systems," Manuscript, Naval Postgraduate School, September 1998.

2. Shumaker, D.L., Wood, J.T. and Thacker, C.R., "Infrared Imaging System Analysis," *Environmental Research Institute of Michigan*, Ann Arbor, Michigan, 1993.

3. McCartney , E., "Optics of the atmosphere : scattering by molecules and particles," 1980.

4. *AGA Thermovision 780 Operating Manual*, AGA Infrared Systems AB, Publication n° 556 556 492, Ed II, 1980.

5. Kneizys, F.X., Shettle, E.P., Gallery, W.O., Chetwynd, J.H., Abreu, L.W., Selby, J.E.A., Clough, S.A. and Fenn, R.W., "Atmospheric Transmittance/Radiance : Computer Code LOWTRAN 6," *Air Force Geophysics Laboratory*, AFGL-TR-83-0187, Hanscom, MA, 01731, 1983

6. Mermelstein, M.D., Shettle, E.P., Takken, E.H. and Priest, R.G., "Infrared Radiance and Solar Glint at the Ocean-Sky Horizon," *Applied Optics*, vol. 33, n° 25, September 1994.

7. Karavas, P., "Validation/Evaluation of Polarization Version of SeaRad Model," Master's Thesis, Naval Postgraduate School, June 1999.

8. Pontes, M.C., "Polarization Effects on Infrared Target Contrast," Master's Thesis, Naval Postgraduate School, September 1998.

9. Cox, C. and Munk, W., "Slopes of the Sea Surface Deduced from Photographs of Sun Glitter," *Scripps Institution of Oceanography Bulletin*, vol. 6, pp. 401, 1956.

10. Jong, A., "Multispectral Maritime Background and Clutter Effects on Small Surface Target Detection," *SPIE Proceedings*, vol. 2742/267, 1996.

11. Bell, E.E., Eisner, L., Young, J. and Oetjen, R., "Spectral Radiance of Sky and Terrain at Wavelengths between 1 and 20 Microns," *Journal of the Optical Society of America*, vol. 50, pp. 1317, 1960.

12. *PTRWIN User's Manual*, CEDIP, 19 Boulevard Georges Bidault, Croissy, Beaubourg, October 1995.

## INITIAL DISTRIBUTION LIST

No. Copies

1. Defense Technical Information Center ..... 2
   87725 John J. Kingman Rd., STE 0944
   Ft. Belvoir, VA 22060-6218

2. Dudley Knox Library ..... 2
   Naval Postgraduate School
   411 Dyer Rd.
   Monterey, CA 93943-5101

3. Engineering and Technology Curricular Office ..... 1
   Code 34
   Naval Postgraduate School
   Monterey, CA 93943-5107

4. Professor William B. Maier II, Code PH/Mw ..... 2
   Chairman, Department of Physics
   Naval Postgraduate School
   Monterey, CA 93943-5117

5. Professor Alfred W. Cooper, Code PH/Cr ..... 3
   Department of Physics
   Naval Postgraduate School
   Monterey, CA 93943-5117

6. Professor Ron J. Pieper, Code EC/Pr ..... 1
   Department of Electrical and Computer Engineering
   Naval Postgraduate School
   Monterey, CA 93943-5121

7. Professor X. K. Maruyama, Code PH/My ..... 1
   Department of Physics
   Naval Postgraduate School
   Monterey, CA 93943-5121

8. Naval Sea Systems Command ..... 1
   PEO – Expeditionary Warfare
   ATTN: Mr. J.E. Misanin, NC2 – Rm. 12 E52
   2531 Jefferson Davis Highway
   Arlington, VA 22242-5170

9. Space and Naval Warfare Systems Center - SD ..... 1
Propagation Division
ATTN: Dr. J.H. Richter, Code D88
53570 Silvergate Ave.
San Diego, CA 92152-5230

10. Space and Naval Warfare Systems Center - SD ..... 1
RDT&E Division
ATTN: Dr. D.R. Jensen, Code D833
53570 Silvergate Ave.
San Diego, CA 92152-5230

11. Space and Naval Warfare Systems Center - SD ..... 1
RDT&E Division
ATTN: Dr. C.R. Zeisse, Code D883
53570 Silvergate Ave.
San Diego, CA 92152-5230

12. Naval Air Warfare Center ..... 1
Research and Technology Group, Physics Branch
ATTN: Dr. J. Bevan
China Lake, CA 93555-6100

13. Roberto Tsustsui, Lieutenant Colonel ..... 1
Instituto de Aeronáutica e Espaço – IAE
Centro Técnico Aeroespacial
12228-904 – São José dos Campos – São Paulo -Brazil